Department of Mechanical Engineering

Sensing the tyre-road contact by intelligent tyre

Arto Niskanen

Aalto University

DOCTORAL DISSERTATIONS

Aalto University publication series
DOCTORAL DISSERTATIONS 129/2017

Sensing the tyre-road contact by intelligent tyre

Arto Niskanen

A doctoral dissertation completed for the degree of Doctor of Science (Technology) to be defended, with the permission of the Aalto University School of Engineering, at a public examination held at the lecture hall M1 (Otakaari 1) on 27th of July 2017 at 12:00.

Aalto University
School of Engineering
Department of Mechanical Engineering
Vehicle Engineering

Supervising professor
Professor Kari Tammi, Aalto University

Thesis advisor
D.Sc. (Tech.) Ari Tuononen, Aalto University

Preliminary examiners
Professor Manfred Plöchl, TU Wien, Austria
Dr. Malal Kane, IFSTTAR, France

Opponent
Professor Jörg Wallaschek, Leibniz Universität Hannover, Germany

Aalto University publication series
DOCTORAL DISSERTATIONS 129/2017

ISBN 978-952-60-7518-1 (printed)
ISBN 978-952-60-7517-4 (pdf)
ISSN-L 1799-4934
ISSN 1799-4934 (printed)
ISSN 1799-4942 (pdf)
http://urn.fi/URN:ISBN:978-952-60-7517-4

Unigrafia Oy
Helsinki 2017

Finland

441 697
Printed matter

Aalto University

Abstract

Aalto University, P.O. Box 11000, FI-00076 Aalto www.aalto.fi

Author
Arto Niskanen

Name of the doctoral dissertation
Sensing the tyre-road contact by intelligent tyre

Publisher School of Engineering

Unit Department of Mechanical Engineering

Series Aalto University publication series DOCTORAL DISSERTATIONS 129/2017

Field of research Vehicle Engineering

Manuscript submitted 26 April 2017 **Date of the defence** 27 July 2017

Permission to publish granted (date) 16 June 2017 **Language** English

☐ **Monograph** ☒ **Article dissertation** ☐ **Essay dissertation**

Abstract

Significant effort has been made in the development of tyres and vehicles to optimize the safety, performance and economy in transportation. Throughout the vehicle development processes, the tyre is considered as a key component for the vehicle behaviour. However, the tyre-road contact is not being measured directly in the production vehicles even though it is the most important part of the vehicle dynamics providing all the forces to control a vehicle. Especially the autonomous vehicles require a reliable estimate of road friction potential for safe operation in varying conditions.

Intelligent tyre research is aiming for sensing the tyre-road contact with different sensors embedded in the tyre. Accelerometers are potential production tyre sensors as well as powerful research tools for tyre development. In this thesis, a tyre with accelerometers mounted on the inner liner is used to study the effects of aquaplaning and friction potential on the measured accelerations.

Accelerometer tyre measurements were conducted with traditional high-speed imaging on a liquid covered glass plate to study aquaplaning. The contact lengths determined from the tangential acceleration showed clearly the shortening of the contact due to the hydrodynamic lift. In addition, the distorted contact shape was visible with both methods. It is shown that the accelerometer tyre can provide powerful tool for the tyre aquaplaning research on real road surfaces. In addition, a method to detect the presence of water in the contact from the lateral acceleration signal was suggested vehicle safety systems in mind.

A simplified flexible ring model was utilized for interpreting the radial acceleration data. The acceleration profile derived from the model could be used to remove the effect of contact deformation from the measured signal dominating the effects of more subtle phenomena such as friction potential. Difference in the contact mechanism on different surfaces were observed from the estimated model parameters and a reliable way to estimate the contact length was obtained by using the model-based approach.

The effects of friction potential were studied on equally smooth surfaces with different friction levels as well as on real road surfaces with varying roughness, friction and deformability levels. First, the vibration in the pre-contact part was found to exist on low-friction surface excited by the local sliding of the tread. On real road surfaces, the surface roughness dominates this effect and Hilbert-Huang transform was utilized to detect even more subtle vibration in the contact. The local sliding was found to occur inside the contact resulting in low-amplitude high-frequency vibration. This was observed on the freely rolling tyre, which highlights the potential of tyre sensing.

The thesis presents methods and applications for utilization of accelerometer as a tyre sensor

Keywords Intelligent tyre, tyre-road contact, accelerometer, aquaplaning, friction potential

ISBN (printed) 978-952-60-7518-1 **ISBN (pdf)** 978-952-60-7517-4

ISSN-L 1799-4934 **ISSN (printed)** 1799-4934 **ISSN (pdf)** 1799-4942

Location of publisher Helsinki **Location of printing** Helsinki **Year** 2017

Pages 122 **urn** http://urn.fi/URN:ISBN:978-952-60-7517-4

Tekijä
Arto Niskanen

Väitöskirjan nimi
Rengas-tiekontaktin aistiminen älykkäällä renkaalla

Julkaisija Insinööritieteiden korkeakoulu

Yksikkö Koneenrakennustekniikan laitos

Sarja Aalto University publication series DOCTORAL DISSERTATIONS 129/2017

Tutkimusala Koneenrakennustekniikka

Käsikirjoituksen pvm 26.04.2017 **Väitöspäivä** 27.07.2017

Julkaisuluvan myöntämispäivä 16.06.2017 **Kieli** Englanti

☐ **Monografia** ☒ **Artikkeliväitöskirja** ☐ **Esseeväitöskirja**

Tiivistelmä

Rengas on olennainen osa ajoneuvoa ja siten myös liikenneturvallisuutta. Rengas-tiekontaktia ei kuitenkaan tuotantoautoissa mitata suorasti, vaikka se on tärkein ajodynamiikkaan vaikuttava asia tuottaen tarvittavat voimat ajoneuvon hallitsemiseen. Erityisesti autonomiset ajoneuvot tarvitsevat tietoa rengas-tiekontaktista, tärkeimpänä tietona kitkapotentiaali, joka mahdollistaa turvallisen toimimisen vaihtelevissa olosuhteissa.

Älykkäisiin renkaisiin liittyvän tutkimuksen tavoitteena on tuottaa tietoa rengas-tiekontaktista anturoidulla renkaalla. Kiihtyvyysanturit ovat potentiaalisia vaihtoehtoja tuotantorengasantureiksi ja tehokkaita työkaluja renkaan kehitystyössä. Tässä väitöskirjassa käytetään kiihtyvyysanturillista rengasta vesiliirron ja tienpinnan kitkapotentiaalin vaikutusten mittaamiseen.

Vesiliirtotutkimuksessa käytettiin kiihtyvyysanturillisen renkaan lisäksi perinteistä suurnopeuskuvausta nestepäällysteisellä lasilevyllä. Renkaan pituussuuntaisesta kiihtyvyyssignaalista määriteltyjen kontaktipituuksien lyheneminen hydrodynaamisen nosteen takia oli selvästi nähtävissä. Myös kontaktin muodon muuttuminen veden vaikutuksesta havaittiin molemmilla metodeilla. Työssä osoitetaan kiihtyvyysanturillisen renkaan olevan tehokas työkalu vesiliirtotutkimuksessa todellisilla tienpinnoilla. Lisäksi esitetään metodi veden tunnistamiseen kontaktissa sivuttaisesta kiihtyvyyssignaalista ajoneuvojen turvallisuusjärjestelmiä silmällä pitäen.

Rengasmallia käytettiin radiaalisuuntaisen kiihtyvyyssignaalin tulkitsemiseen ja sen avulla saatu tiekontaktista aiheutuva kiihtyvyysprofiili voitiin poistaa mitatusta kiihtyvyyssignaalista. Tällöin jäljelle jäävää signaalia voidaan käyttää hienovaraisempien ilmiöiden, kuten kitkapotentiaalin havaitsemiseen. Estimoiduista malliparametreista voitiin havaita erilaiset kontaktimekanismit erilaisilla tienpinnoilla ja kontaktipituudet saatiin luotettavasti mallipohjaisella lähestymistavalla.

Kitkapotentiaalin vaikutusta mitattuihin kiihtyvyyksiin tutkittiin sekä erittäin tasaisilla pinnoilla, että todellisilla tienpinnoilla joilla oli erilaiset pinnankarheus-, kitka- ja muokkautuvuusominaisuudet. Makrokarheudeltaan yhtenevien pintojen tapauksessa voitiin havaita ennen kontaktin tuloreunaa esiintyvä, paikallisesta kumin liukumisesta aiheutuva suurempi värähtely liukkaalla pinnalla. Todellisilla tienpinnoilla pinnankarheuden aiheuttama värähtely dominoi tuloreunalla. Hilbert-Huang-muunnosta hyödyntämällä havaittiin ja paikallistettiin kontaktin sisällä tapahtuva paikallinen liukuminen ja sen aiheuttama korkeataajuuksinen ja matala-amplitudinen värähtely liukkailla pinnoilla, joka voitiin erottaa pinnankarheudesta johtuvasta värähtelystä. Tämä paikallinen liukuminen voitiin havaita vapaasti pyörivässä renkaassa, mikä alleviivaa rengasanturoinnin tuomia mahdollisuuksia.

Avainsanat Älykäs rengas, rengas-tiekontakti, kiihtyvyysanturi, vesiliirto, kitkapotentiaali

ISBN (painettu) 978-952-60-7518-1 **ISBN (pdf)** 978-952-60-7517-4

ISSN-L 1799-4934 **ISSN (painettu)** 1799-4934 **ISSN (pdf)** 1799-4942

Julkaisupaikka Helsinki **Painopaikka** Helsinki **Vuosi** 2017

Sivumäärä 122 **urn** http://urn.fi/URN:ISBN:978-952-60-7517-4

Acknowledgements

The research for this dissertation was carried out in the Vehicle Engineering research group at Aalto University.

First, I would like to thank my instructor Dr. Ari Tuononen for all the input to this thesis and most of all the ambitious and inspirational way of leading the research group. I would also like to express my gratitude to my supervisor Prof. Kari Tammi for the support and guidance. Sincere appreciation goes to my preliminary examiners Dr. Malal Kane and Prof. Manfred Plöchl. It is an honour to have Prof. Jörg Wallaschek as my opponent in the public defence of this dissertation.

The help and inspiration I have received from the colleagues inside and outside the Vehicle Engineering laboratory is acknowledged. The atmosphere in the research group has always been supporting and inspiring. Leaving many names unmentioned shall be considered as an equal and sincere appreciation for everyones input. For my fellow doctoral students Mona, Yi and Andras, thank you for making the journey unforgettable.

No words can describe the importance of my family and their support throughout a much longer period than my doctoral studies. The last words I dedicate to my dear Liisa, this achievement would not matter without you.

Espoo, June 2017

Arto Niskanen

Contents

List of Symbols

a	unloaded tyre radius
a_{ins}	instantaneous amplitude
A_{pc}	indicator for pre-contact vibration
A_c	indicator for contact vibration
b	belt width
c	equivalent damping
c_v	damping in tangential direction
c_w	damping in radial direction
h	proto-IMF
k	equivalent spring stiffness
k_v	spring stiffness in tangential direction
k_w	spring stiffness in radial direction
l	lower envelope
m	mean envelope
p	nominalized inflation pressure
p_o	inflation pressure
u	upper envelope
v	tangential deformation
w	radial deformation
w_f	pre-contact radial deformation
w_r	after-contact radial deformation
x	original signal
y_{filt}	band-pass filtered lateral acceleration signal
z	analytic signal

θ	phase function
ω	instantaneous frequency
Ω	wheel rotational speed
δ	maximum radial deformation
φ	wheel rotation angle
φ_f	leading edge angle
φ_r	trailing edge angle

List of Abbreviations

ABS	Anti-lock Brake System
ACC	Adaptive Cruise Control
AEB	Autonomous Emergency Brake
DAQ	Data Acquisition
EMD	Empirical Mode Decomposition
ESC	Electronic Stability Control
HHT	Hilbert-Huang Transform
HSA	Hilbert Spectral Analysis
IEPE	Integrated Electronic Piezoelectric
IMF	Intrinsic Mode Function
LED	Light-Emitting Diode
PCA	Principal Component Analysis
PV	Principal Value
SAW	Surface Acoustic Wave
TPMS	Tyre Pressure Monitoring System
V2X	Vehicle-to-Everything

List of Publications

This doctoral dissertation consists of a summary and of the following publications which are referred to in the text by their numerals

I. Niskanen, Arto; Tuononen, Ari. 2014. Three 3-axis accelerometers fixed inside the tire for studying contact patch deformations in wet conditions. Vehicle System Dynamics, 52(1), pp. 287-298. DOI: 10.1080/00423114.2014.898777.

II. Niskanen, Arto; Tuononen, Ari. 2015. Accelerometer tyre to estimate the aquaplaning state of the tyre-road contact. IEEE Intelligent Vehicles Symposium (IV), Seoul, Korea, Jun 28 - Jul 1, pp. 343-348. DOI: 10.1109/IVS.2015.7225709.

III. Niskanen, Arto; Tuononen, Ari. 2015. Three three-axis IEPE accelerometers on the inner liner of a tire for finding the tire-road friction potential indicators. Sensors, 15(8), pp. 19251-19263. DOI: 10.3390/s150819251.

IV. Niskanen, Arto; Tuononen, Ari. 2016. Towards the friction potential estimation: A model-based approach to utilizing in-tyre accelerometer measurements. IEEE Intelligent Vehicles Symposium (IV), Gothenburg, Sweden, Jun 19-22, pp. 625-629. DOI: 10.1109/IVS.2016.7535452.

V. Niskanen, Arto; Tuononen Ari. 2017. Detection of the local sliding in the tyre-road contact by measuring vibrations on the inner liner of the tyre. Measurement Science and Technology, 28(5), pp. 1-12. DOI: 10.1088/1361-6501/aa6148.

Author's Contribution

I The author contributed the planning, preparation and conduction of the measurements together with the co-author. The author conducted the data processing and prepared the analysis of the results. The manuscript was written together with the co-author.

II The author contributed the planning, preparation and conduction of the measurements together with the co-author. The data processing was conducted mainly by the author and the results were analysed and the manuscript written together with the co-author.

III The author planned and conducted the measurements inspired by the co-author. The processing and analysis of the data was conducted by the author. The interpretation of the results and the writing of the manuscript was done together with the co-author.

IV The measurements were planned and conducted by the author and the co-author (Ari Tuononen). The data processing and model fitting procedure was done by the author. The analysis of the results and the writing of the manuscript was conducted together with the co-authors (Ari Tuononen, Yi Xiong).

V The measurements were planned and conducted by the author and the co-author. The author had major contribution to the data processing and the analysis of the results. The manuscript was prepared together with the co-author.

1. Introduction

1.1 Background and motivation

Friction between the tyre and the road is essential for traffic safety. The small area between the tyre and the road generates all the forces needed to control a vehicle. An increasing amount of automatic safety and convenience features such as adaptive cruise control (ACC) and automatic emergency braking (AEB) are introduced in the production cars. These systems would benefit from the the tyre-road contact information enabling them to be proactive. The autonomy of the transportation is increasing rapidly creating a need for better sensing. Especially the upcoming autonomous cars will require a good estimate of the friction conditions to be able to adapt to varying environments. The more accurate and real time the information, the better the response and the safety level achieved.

Even though the current electronic stability control systems (ESC) can rather effectively control a car and have been shown to increase the safety in traffic [1], they still lack the direct friction information from the tyre-road contact. These systems rely on the information from the sensors such as wheel rotational speed sensors, car body acceleration and yaw rate sensors [2]. Sensor information for the control systems thus presents the current state of the car when the conditions in the tyre-road contact have already affected. The elastic nature of the tyre introduces a delay before the contact patch forces are transmitted to the vehicle [3]. The elasticity of the suspension and rubber joints further increase the delay between the forces generated in the contact and the measured car body movement.

In addition to an individual vehicle control system, tyre sensors can provide essential information for the vehicle-to-everything (V2X) communication. Connected cars have emerged the market quickly and the full potential is still to be utilized. Intelligent infrastructure providing cloud-based information is an additional platform, for which tyre sensors could provide information. Road condition and friction potential information being the most intriguing to be distributed for the autonomous vehicles. Moreover, the efficiency of the road maintenance can be improved by obtaining more real-time and localized road information.

Up to this point, tyre sensors have been mostly used for tyre research and development. Intelligent tyres can be powerful tools for the development of tyres. Validation and parametrization of the simulation models, performance testing and modal analysis being few examples of the tasks assigned for the tyre sensors. For such purposes, the cost and robustness of the systems are not an issue

but when aiming for the production tyre sensors, they become significant limitations. The intelligence in production tyres is increasing. The tyre pressure monitoring system (TPMS) required by the legislation being the first step [4] and followed recently by the tyre condition monitoring and cloud-based consumer services [5].

To justify the added cost of the sensors, they need to provide information valuable enough. In addition, the information the sensors provide, need to be reliable and robust to meet the high standards of vehicle safety. The motivation for this thesis rises from the potential, which intelligent tyres have but also from the complexity what is faced with interpreting the data. This thesis provides methods and understanding for interpreting accelerometer data measured on the inner liner of the tyre. The intent is not to develop production-ready algorithms but to provide valuable insight to the phenomena measurable by the accelerometer tyre and thus support the development of intelligent tyres.

1.2 Scope of the thesis

This thesis focuses on the utilization of the accelerometer as a tyre sensor to interpret the state of the tyre-road contact. An effort is made to produce valuable results for the development of intelligent tyres from different aspects. Methods to analyse and utilize the data are introduced and the physical phenomena revealed. The accelerometer data is analyzed with the tyre research and development as well as the vehicle safety and control systems in mind. In addition, the intelligent infrastructure will benefit from the road information and thus, the more computationally demanding methods could be implemented for such purposes. The aspects of the tyre sensor utilization considered in this thesis include aquaplaning and water detection, a model-based tyre sensor data interpretation and the effects of the tyre-road contact friction potential on the measured acceleration from the tyre inner liner.

1.3 Scientific contributions

The thesis contributes in the field of intelligent tyre research by providing unique measurement results from the real road environments, which the tyre sensors are facing and analysis methods to discover the phenomena of interest. The measurements are conducted by utilizing advanced sensors and data acquisition systems. This way the focus is on the detection of the underlying physical phenomena more than on the application based and market-ready system development. The scientific contributions of this thesis can be summarized as follows:

- Unique aquaplaning measurements were conducted by utilizing three accelerometers on the inner liner of the tyre and high-speed imaging to detect the state of the aquaplaning in the contact and the distorted contact shape due to the hydrodynamic pressure. Comparison of these

two methods revealed the suitability of the tyre sensors for the tyre aquaplaning research and development on real road conditions. The information obtained could also be provided for the vehicle safety systems. (in Publication [I])

- A method to detect the contact length in the different phases of the aquaplaning was suggested and an algorithm to detect the water in the tyre-road contact based on the tyre lateral vibration was developed. (in Publication [II])

- The effect of the friction on the measured accelerations near contact patch was revealed by comparing surfaces with the same macro-roughness but different friction levels. Without the effect of the road roughness, the vibration in the pre-contact region, excited by the local sliding at the leading edge was discovered. The area under the band-pass filtered acceleration signal power spectrum was suggested as an indicator of friction potential level on equally macro-smooth surfaces. (in Publication [III])

- A model-based approach for utilizing the tyre sensor data was introduced. A simplified flexible ring model was used as a basis to estimate the parameters of the model by fitting it to the measured acceleration. This provided a method to extract the effect of the contact deformation from the measured acceleration resulting in a physical model-based filtering method for the tyre sensor data. The variation in the estimated parameters suggested different contact boundaries on different surfaces. In addition, the contact length information could be estimated more reliably than with the traditional peak-seeking method. (in Publication [IV])

- The detection of the local sliding from the freely rolling tyre in low friction conditions was further studied by including real road surfaces with varying roughness levels. Utilizing empirical mode decomposition and Hilbert spectral analysis (together called Hilbert-Huang transform), the local sliding could now be detected in the contact. The energy of the tangential vibration in the trailing part of the contact was shown to correlate with the assumed friction level. An increased lateral vibration was detected in the leading part of the contact. The effect of the surface roughness in the pre-contact vibration was discovered to dominate the effect of the friction. (in Publication [V])

2. Intelligent tyres

2.1 Tyre properties

Despite its simple appearance, tyre is a complex composite structure. A typical passenger car tyre consists of carcass, belt and tread. Additional parts can be identified but these are the most essential ones affecting the tyre behaviour. The carcass is the base of the tyre carrying the load and the internal air pressure, allowing flexibility to comply with the road irregularities and transmitting the forces acting on the tyre-road contact to the wheel. The carcass usually has a varying number of layers of cords called plies, which provide the strength against the inflation pressure. These cords are bonded to the carcass rubber. Belt is an essential part of the modern radial tyre being a tangentially rigid layer between the tread and the carcass usually consisting of steel and nylon layers. It provides structural rigidity and resistance to punctures. Belt has a great influence on the modern radial tyre behaviour as will be discussed later on. Tread is the part contacting the road surface and thus very critical for the safety, performance and economy of the tyre. Several requirements are set for the tread design including good dry and wet grip, low rolling resistance and sufficient wear resistance.

As mentioned, the belt has a significant effect on the radial tyre behaviour. It strenghtens the structure by having high tensile strength and provides more stable contact patch [6]. The high tensile strength of the belt leads to a typical assumption of inextensibility when modelling the tyre for example by a well-known flexible ring model [7]. The belt has also a significant effect to contact stress distributions. The understanding of the tyre-road contact stresses is vital for the tyre sensor measurements. This is especially true for the aquaplaning and friction related phenomena considered in this thesis. The stresses considered are the shear stresses (acting in the longitudinal and lateral direction) and the normal stress (acting in the vertical direction).

In aquaplaning, the hydrodynamic pressure of the water layer lifts the tyre from the road starting from the leading edge. The normal pressure distribution is shifted towards the leading edge of the contact. This front-biased pressure distribution can be thought also as a force creating a braking moment to the wheel similar to the rolling resistance. This results in decreasing wheel rotational speed, commonly known as a spin-down, which can lead to a completely stopped wheel near full aquaplaning. Since the tyre structure is stiffer in the shoulder area, the hydrodynamic pressure will deform the centre part of the

contact more since the water can penetrate there more easily. In the centre of the contact, the hydrodynamic pressure is mainly acting against the inflation pressure of the tyre. This is why the tyre pressures should be kept sufficient to prevent the loss of the tyre-road contact in wet conditions. The stiff belt will also reduce the amount of distortion, as it will distribute the pressure in the contact more evenly.

In Figure 1, a simplified longitudinal shear stress distribution for a braking, accelerating and a freely rolling tyre is shown. The freely rolling tyre is generating driving shear stress in the leading part of the contact and braking shear stress in the trailing part of the contact [6], [8]. The point for the change of stress direction is not usually in the middle of the contact length and is dependent on many parameters in the tyre structure such as the hysteresis of the tread rubber and the tread design. The shear stress distribution is contributed by several factors. First, the relaxation of the pretensioned belt when compressed against the road, will introduce a static stress field where the direction of the stress field is pointing towards the edges of the contact due to the tread shrinkage. This is opposite from the stress field pointing towards the centre of the contact, which a solid tyre without air cavity would produce resulting from the Poisson effect. The Poisson effect is however observable in the tread pattern scale in a pneumatic tyre also. An individual tread block compressed against the surface will result in a local stress field pointing towards the centre of the tread block. The longitudinal stress distribution when integrated over the whole contact area will always result in a small negative force, which is the rolling resistance loss due to the viscoelastic behaviour of the tyre rubber. At the trailing edge, the shear stress changes the direction rapidly back from braking shear stress to driving shear stress as indicated by the dashed circle in Figure 1. This has been explained by the viscous property of the rubber when the belt is bending and deflecting the tread block at the trailing edge [9].

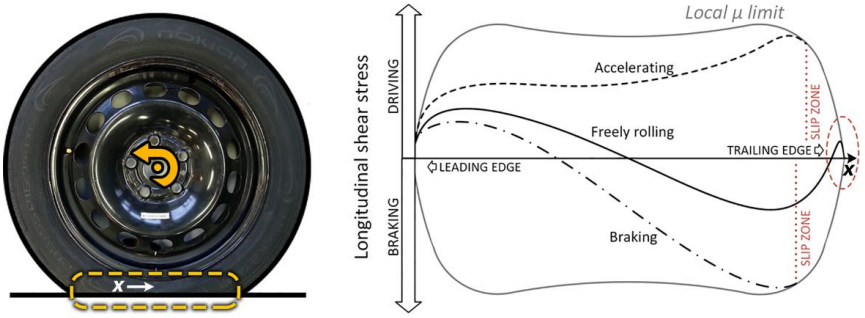

Figure 1. The longitudinal shear stress distribution of a braking, accelerating and freely rolling tyre in the contact patch.

When driving or braking forces are applied, the stress distribution will be altered. The shear stress curve is shifted to the corresponding direction. In moderate braking, the leading part of the contact still operates under driving shear stress. When increasing the braking effort, the trailing part of the contact will

first exceed the friction limit defined by the normal stress and the friction coefficient. When accelerating, the whole contact will earlier become under driving shear stress and the friction is utilized more evenly throughout the contact [10].

The lateral shear stress distribution is similar to the longitudinal one since the belt is also pretensioned in the lateral direction forming a curvature. The relaxation of this pretension leads to a stress field comparable to the longitudinal one where the direction is towards the edges of the contact patch. The Poisson effect is again a contributor especially, when considering longitudinal tread ribs. The ribs will produce a lateral stress field where the direction is pointing towards the center of the rib. In addition, the lateral stress field is affected by the camber angle.

Rotating tyre introduces phenomena, which should be considered when utilizing tyre sensor measurements. The co-rotating accelerometer is affected by fictitious forces, i.e. the Coriolis force, Euler force and centrifugal force. The Euler force is due to the change in the rotational speed of the reference frame and can be omitted in the case of constant tyre rotational speed. The Coriolis force causes the coupling of the radial and tangential acceleration. The bifurcation of the natural frequencies for the forward and backward travelling waves of the same wave number is an effect due to the Coriolis force [11]. The centrifugal force increases the pretension of the belt and results in increased propagation speed of the bending waves in the tyre [11]. In addition, the centrifugal acceleration is obviously detected with the accelerometer in a rotating tyre. The Doppler shift is also a noticeable effect in a rotating tyre sensor measurement. For a co-rotating accelerometer, the road contact acts as a moving excitation source. Thus, the frequencies observed at the leading and trailing edge are subjected to Doppler shift, which results in higher frequencies measured at the leading edge. The effect is rather linear and related to the speed of the propagating wave and the rotational speed of the tyre [12]. This can be taken into consideration where needed.

2.2 Tyre sensing

Tyre sensors have been actively studied in the last few decades. However, no intelligent tyre application has emerged into production car market, excluding the tyre pressure monitoring systems (TPMS). The ability to monitor the tyre-road contact and measure the friction potential is without a doubt the most appealing feature a tyre sensor can provide. The present advanced driver assistance systems (ADAS) such as adaptive cruise control (ACC) and autonomous emergency braking (AEB) would benefit by being able to adjust the safety gap based on the friction information. More importantly, the autonomous vehicles will require a constant and reliable estimate of friction to be able to operate safely in all operating conditions. Throughout the history of intelligent tyre research, various sensor types have been used to measure the state of the tyre indicating the underlying operating conditions.

Several requirements are given for a tyre sensor due to its operating environment. The sensor should not affect the tyre structure significantly. This includes

the requirement for balancing the rotating tyre if significant mass is introduced by the sensor unit. In addition, the deformation of the tyre should not be affected by the sensor resulting in heterogeneous behaviour. The data transmission between the vehicle and the tyre poses a challenge if high data transfer rates are required. High data rates require significant amount of energy, which need to be provided to the rotating tyre. This is usually implemented by using slip ring, battery, energy harvesting devices or passive sensor elements. For research purposes, any of these methods work but for production vehicles, the requirements are stricter. The energy harvesting devices have been shown to be able to provide energy for the low data rate sensors such as TPMS [13]. However, they cannot provide constant power supply for high data rate sensors such used in this thesis. In addition, the harsh environment and extreme loads the tyre suffers, make the sensor selection challenging.

The Darmstadt tyre sensor [14] can be considered one of the first implementations in the field of intelligent tyres. It comprises of a magnet vulcanized into a tread element and Hall sensors mounted on the tyre inner liner. By measuring the changes in the voltage induced by the magnet, its position and thus the deformation of the tread element can be calculated.

After the Darmstadt tyre sensor, deformations and strains in the tyre has been investigated with variety of sensor types. Tyre forces can be estimated by measuring the torsion of the sidewall. This can be achieved by attaching magnetic markings to the sidewall and measuring the magnetic field with magnetoresistive sensors mounted in the suspension [15]. Surface acoustic wave (SAW) sensors provide a passive way to sense the tyre [16], [17]. SAW sensors are read from outside the tyre by providing a radio frequency signal, which is reflected back from the sensor. The reflected signal is altered by the impedance change in the sensor due to the deformation. By measuring this change, the deformation of the tyre can be obtained. These sensors do not need power supply in the tyre, which is a significant benefit. An approach where the tyre itself is utilized as a sensor was introduced in [18]. The steel wires in the tyre belt act as a capacitor in a capacitance-resistance circuit. The deformation in the tyre changes the capacitance and thus the frequency of the oscillation in the circuit. By observing the changes in the frequency, the deformation of the tyre could be obtained. The fundamental idea of utilizing the tyre components without adding external sensors is intriguing. Yet, the strain-frequency relation can be highly dependent on the individual tyre and its condition.

Optical tyre sensors have been proved very accurate and powerful tools for the tyre research and development. Position sensitive detector mounted on the rim and a light-emitting diode (LED) attached on the inner liner of the tyre was used in [19]–[21]. The deformation of the tyre could be measured based on the light intensity changes in the detector. However, the orientation of the LED changes during the tyre-road contact resulting in challenges interpreting the light intensity measurements. Further studies have employed a laser sensor requiring no components to be attached to the inner liner of the tyre to measure the radial deformation. A spot laser and a line laser sensor has been utilized. The spot laser can be used to measure the radial deformation accurately in one circumferential

line [22], [23] whereas the line laser can scan the contact area and reveal asymmetric radial deformation also in lateral direction [24], [25]. Camera has also been used to detect the inner liner strain and displacement [26] as well as to detect the longitudinal slip ratio from outside the tyre [27].

All the previous mentioned approaches have been successfully utilized in the tyre research. However, two main requirements can be considered essential for the tyre sensor to be viable for production. The first is the cost and manufacturing point of view: can it be manufactured so that it survives the tyre lifetime, can communicate with the vehicle and is still cost-efficient? The second point of view is the usefulness: what can be measured and is the information beneficial enough to be implemented. The accelerometer has shown exceptional potential to become the first actual production-ready tyre sensor fulfilling the before mentioned requirements in addition to TPMS. The accelerometers are widely used in research and industry. They can be extremely robust, small-sized and cost-efficient. The measured physical quantity, acceleration, can be related to many phenomena acting in the tyre. It can be used to detect vibration and by double integral, the contact deformation can be obtained.

Various studies with different approaches have been conducted by using accelerometer as a tyre sensor. One of the first published in-tyre accelerometer implementations studied the fundamental behaviour of the rolling tyre including vibration and radial deformation [12]. Being widely used in vibration measurements, the accelerometer has also been utilized to conduct operational modal analysis of rotating tyres [28]. It provides simpler and cheaper way to conduct the measurements than the typically used laser Doppler vibrometer. Tyre vibration has also a major role in the tyre noise generation. The correlation between the vibration and the wheel-slap noise was studied in [29] by utilizing accelerometer mounted in the tread groove. With in-tyre accelerometer, the effect of the tread block dynamics on the measured acceleration on the inner liner has been researched experimentally [30], [31]. These studies have shown the correlation between the high-frequency vibration and the tread block dynamics. In addition to vibration, the contact deformation has also been of interest in accelerometer studies. Tyre sideslip angle has been estimated based on the measured lateral deformation of the tyre in the contact patch by double integrating the acceleration signal [32], [33]. By utilizing a tyre model, estimates of tyre forces and friction can be obtained. In a similar way, radial and longitudinal forces have been estimated from the acceleration signal. The radial forces can be estimated from the contact length change and the longitudinal forces from the phase shift between the contact angle and the wheel encoder angle as the tyre windup occurs [34]. This idea was further investigated by utilizing principal component analysis (PCA) and reducing the signal into few linear projections, which correlate with the tyre forces [35]. Application for road monitoring and road classification with intelligent tyre has been developed [36]. The basis of the classification is the frequency analysis of the tyre vibration. Additional sensors such as microphone has also been used to improve the accuracy of the classification [37].

A common factor for many tyre sensing approaches is the ability to estimate or classify specific variables in specific conditions with specific equipment. When operating conditions change significantly (e.g. temperature, tyre pressure, tyre wear level), the methods fail to produce usable information. The application-based development has been labelling the intelligent tyre research to some extent. Certainly tyre-optimized equipment and methods are required when reliable information for vehicle control systems is produced. However, the underlying phenomena are common to the tyre-road contact in larger scale. Understanding of these phenomena and their effect on tyre sensor information is the key to successful utilization.

3. Tyre with accelerometer

3.1 Measurement setups

The three-axis accelerometer model used in the measurements was Endevco 35A Isotron [38]. It is an integrated electronic piezoelectric (IEPE) type sensor with a measurement range of ±1000 g. The accelerometer is AC coupled so that the DC component of the signal is removed, and thus for example the constant centrifugal acceleration is not measured. The sensor weighs only 1.1 grams and the dimensions are 7.62 x 6.35 x 6.35 mm. This sized sensor has a negligible effect on the tyre structure, which is essential for the tyre sensors as discussed earlier. The accelerometer was glued to the inner liner with cyanoacrylate adhesive. The sampling rate for the acceleration signal was 25.6 kHz for all the measurements. The coordinate system for the accelerometer axes is shown in Figure 2 and Figure 3. The accelerations in X-, Y- and Z-axis are also called the tangential, lateral and radial acceleration respectively.

The accelerometer model was the same in all of the measurements. For the aquaplaning measurements (Publications [I & II]), three accelerometers were used and mounted side-by-side to cover the half of the contact width as shown in Figure 2. This setup was also used for the friction study on equally smooth surfaces (Publication [III]). The first sensor located behind a longitudinal rib in the center. The second sensor was located behind a rib next to the centremost one (closer to the outside shoulder of the tyre). This rib was slightly narrower than the one in the centre. The third sensor was mounted behind a tread block on the outer shoulder part of the tyre. The tyre was Nokian Hakka Z (205/55R16).

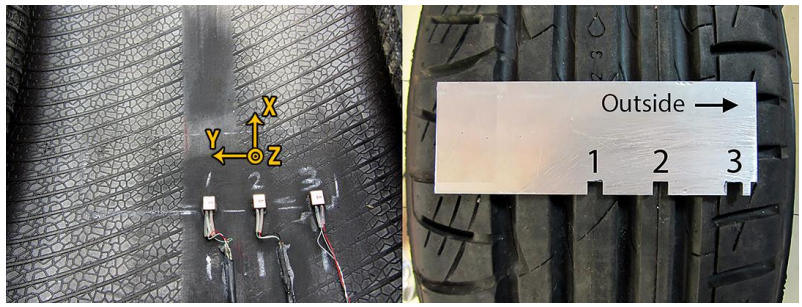

Figure 2. Three accelerometers mounted on the inner liner covering the half of the contact width and the coordinate system for the accelerometers (left). Accelerometer locations visualized in the contact patch (right).

The measurement setup for the real road friction measurements (Publication [V]) is shown in Figure 3. The data obtained with this setup was also used in the model-based approach presented in Publication [IV]. The tyre used in these measurements was Nokian Hakka Green (205/55R16) and one accelerometer was mounted on the inner liner. The accelerometer was located behind the centremost longitudinal tread rib and between the shallow lateral grooves in the rib. The coordinate system of the accelerometer is also shown in Figure 3. The quality of the measured data further improved in the new setup due to the different IEPE-amplifier, tyre inner liner and improved wiring.

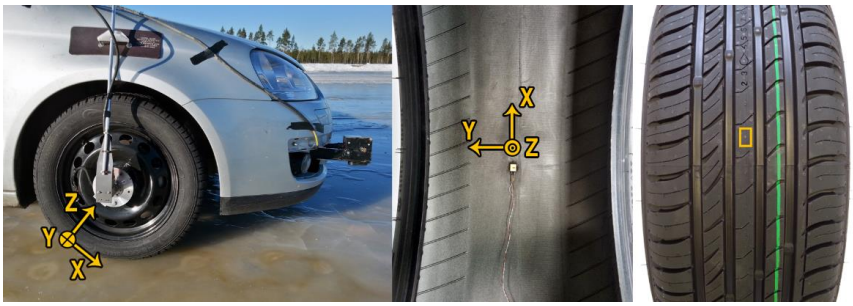

Figure 3. Instrumented car with the slip ring, wheel encoder and optical speed sensor (left). Tyre with the accelerometer mounted on the inner liner (centre). Accelerometer location visualized in the contact patch (right).

The accelerometer tyre was mounted on an instrumented Volkswagen Golf V passenger car (see Figure 4). A special rim was used including an airtight flange with connectors for the accelerometer wiring. The excitation current for the sensors and the signal from the sensors were transmitted then through a slip ring. The slip ring had an in-built wheel encoder, which was used to measure the wheel angle and the rotational speed. National Instruments data acquisition (DAQ) chassis and modules were used to log the data. Analog, digital, CAN-bus and IEPE-modules were used. The accelerometers were read by NI 9234 and NI 9232 analog input modules with IEPE signal conditioning. The vehicle speed was measured by Correvit S-350 Aqua optical speed sensor.

Figure 4. Measurement wheel with airtight flange with connectors for accelerometer wiring (left). Instrumented VW Golf V equipped with optical speed sensor, slip ring, and the accelerometer tyre (right).

3.2 Measurements

The aquaplaning measurements were conducted on a special proving ground including a water pool with a controlled depth of water and a glass plate for high-speed imaging. The glass plate was filled with liquid and the depth was comparable to the water depth of the water pool (8 mm). A high-speed camera was mounted below the glass plate so that the runover could be recorded. The resolution of the camera was 1024 x 1024 pixels and the frame rate 2000 frames per second. Before the water pool section, there was a dry asphalt straight, which was also used to obtain data. Triggering points were used to separate the data between the sections during data processing.

The measurement procedure was as follows. First, the car was accelerated to the measurement speed and driven over the glass plate for high-speed imaging. With the same speed, the car was driven first through the dry asphalt section followed by the water pool to obtain the data from the accelerometers. The clutch was disengaged before entering the dry asphalt section so that the tyre was freely rolling (except the speeds of 20 km/h and below when the clutch was engaged to provide enough traction to manage through the measurement). The high-speed imaging and the accelerometer measurement were conducted thus in separate sections but on the same measurement run. The procedure was repeated with different tyre pressures and driving speeds. Critical aquaplaning speeds for different tyre pressures were determined in a separate test in which the car was accelerated near the full aquaplaning speed. The speed of the vehicle at the time when the wheel rotational speed rapidly increased was recorded as the critical speed. The data from these measurements were used in Publications [I & II].

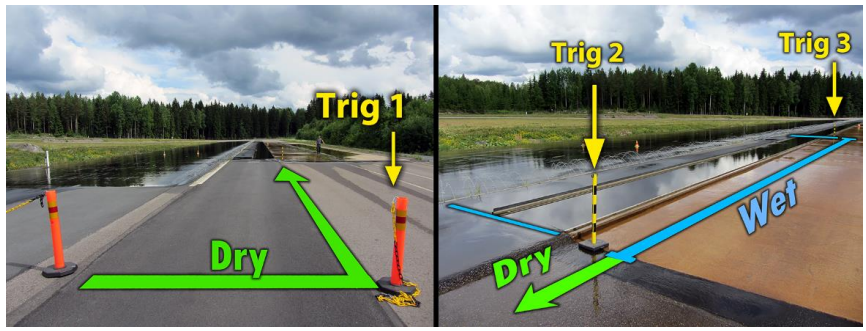

Figure 5. The test track for the aquaplaning measurements containing dry asphalt section and the water pool section.

Next, the effect of friction level on the measured acceleration on the inner liner was researched. To study the pure frictional phenomena, two equally macro-smooth surfaces with different friction levels were chosen to remove the surface roughness effect on the measured signal. The surfaces were smooth ice, and smooth concrete as show in Figure 6. Driving speeds were limited to 10, 20 and 30 km/h due to the test site limitations. The car was accelerated to the test speed and the clutch was disengaged before the measurement started. Three different

tyre pressures were tested: 2.2, 2.4 and 2.6 bar. The data from these measurements were used in Publication [III].

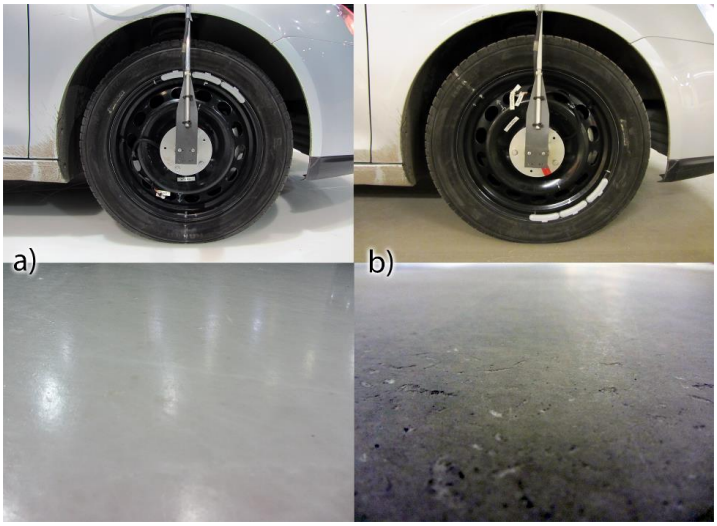

Figure 6. Two equally macro-smooth surfaces with different friction levels used in Publication [III]. (a) Smooth ice and (b) smooth concrete.

The final measurements were conducted on a proving ground used for vehicle testing. This time real road conditions were used for the measurements including asphalt, smooth ice, rough ice and snow surfaces. The asphalt surface was comparable to a typical Nordic road in good condition. The smooth ice was comparable to a frozen lake surface with smooth macro-roughness. The rough ice represented frozen asphalt surface with more sharp roughness on the top. The snow surface was packed snow comparable to a ploughed snow road. With these test surfaces, the friction, roughness and deformability effect of the surface on the measured acceleration could be considered. The rough ice was rougher than the asphalt and on the other hand, the friction was lower. By having also the smooth ice surface, the friction and roughness effects could be separated. The snow surface differs greatly from the three other surfaces since it is highly deformable compared to the others. This results in significantly different contact mechanism. A visualization of the properties of the used surfaces is shown in Figure 7. The effective roughness in this case indicates the surface roughness affecting mainly the vibration of the tyre (i.e. macro-roughness). The data from these measurements were used in Publications [IV & V].

3.3 Methods

To interpret the tyre sensor data, multiple data processing methods have been utilized. Efficient filtering and frequency analysis methods are needed to reveal the phenomena of interest from the acceleration signals.

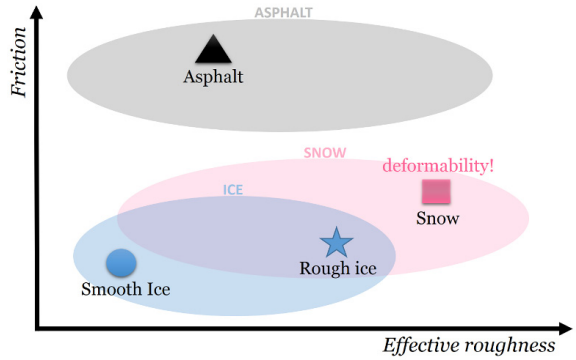

Figure 7. Typical friction and roughness levels for the three different surface types marked with the transparent areas. Relative friction level and surface roughness for the four real road test surfaces used in Publication [IV & V] marked with the symbols.

3.3.1 Aquaplaning

The following section describes the methods used in Pulication [I]. The tyre-road contact length is determined based on the tangential acceleration signal. After zero-phase Butterworth low-pass filtering the signal, the acceleration waveform shows two or three peaks depending on the contact conditions. The detection of the peaks from the filtered signal is conducted by finding points where the derivative of the signal goes to zero. In the case of partial aquaplaning (see Figure 8 (a)), three prominent peaks are present. The first negative peak is assumed to indicate the moment when the sensor part of the tyre hits the water. This is followed by another negative peak when the tyre comes in contact with the road surface. The third positive peak indicates the sensor leaving the contact. The section between the first two peaks is the hydrodynamic region where the hydrodynamic forces of the water dominates. The tyre forces are transmitted to the road through the weak viscous forces of the water layer in this region. The other section between the second and third peak is presenting the viscous or wet contact region. In this region, the tyre is in contact with the road but a thin layer of liquid is present. The viscous properties of the liquid determines how easily the tread can squeeze the liquid away from the contact. However, this region is the main contributor for the tyre force generation. Since the trailing part of the contact is creating most of the tyre forces in this case, the aligning moment transmitted through the steering wheel can give the driver a misleading feel of grip until it is completely lost.

In the full aquaplaning, the tyre is completely lifted away from the road contact. In this case, there are practically no tyre forces transmitted to the road except the weak viscous forces. The low-pass filtered accelerometer signal shows two peaks (see Figure 8 (b)) as in the case of normal dry contact. However, the raw signal shows clear indication of water present in the contact. Significant vibration can be detected throughout the contact due to the water layer turbulence.

The coloured bars are located above the high-speed images by visually inspecting the detachment of the centremost tread rib from the contact at the trailing

edge. Thus, it is the contact length information from accelerometer 1 that is first located over the high-speed image and the two other contact lengths from the accelerometer 2 and 3 added with corresponding phase shift as observed from the time-domain signals. The difference in time between the trailing edge peaks from the sensors are transformed into distance by multiplying the time with the speed of the wheel. Now the coloured bars are indicating not only the contact lengths but also the relative difference in distance when the contact on each sensor location occurred.

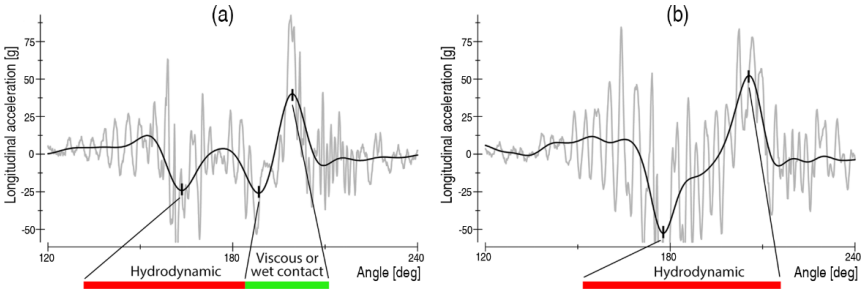

Figure 8. Contact length determination method for (a) partial aquaplaning and (b) full aquaplaning. The dark solid line is the filtered signal and the markers show the detected peak values. The red and green bars show the identified contact lengths that are shown in the results section.

3.3.2 Water detection

In Publication [II], the aquaplaning measurement data is further processed. The detection of the leading and trailing edge is once again done by seeking the peaks (i.e. derivative is zero) of the filtered tangential acceleration. Filtering method is slightly improved from the Publication [I] by applying third order zero-phase Butterworth band-pass filter. A fixed lower limit of 10 Hz is used to remove the non-contact-related low-frequency components. A moving upper limit of 75 - 400 Hz is used for driving speeds of 20 - 100 km/h respectively.

To detect the presence of water in the tyre-road contact, the lateral acceleration signal is utilized. Since the normal excitation from the road contact is lowest in the lateral direction, all external excitation produce rather noticeable difference. This is the case also with the turbulent water flow in the contact. A band-pass filtering routine similar to the contact length detection is implemented for the lateral acceleration signal to separate the frequencies excited by the water. A moving lower limit of 300 – 1000 Hz for driving speeds of 20 – 100 km/h respectively and a fixed upper limit of 2000 Hz is used. The filtered acceleration signal is then divided into pre-contact and contact sections as shown in Figure 9.

The absolute values of the filtered signals are integrated over these two sections to obtain quantitative indicators of the vibration. For the pre-contact section, the integral with respect to the rotation angle of the wheel φ is done between the point x_{pc} and x_{c1}:

$$A_{pc} = \int_{x_{pc}}^{x_{c1}} |y_{filt}(\varphi)| d\varphi \tag{3.1}$$

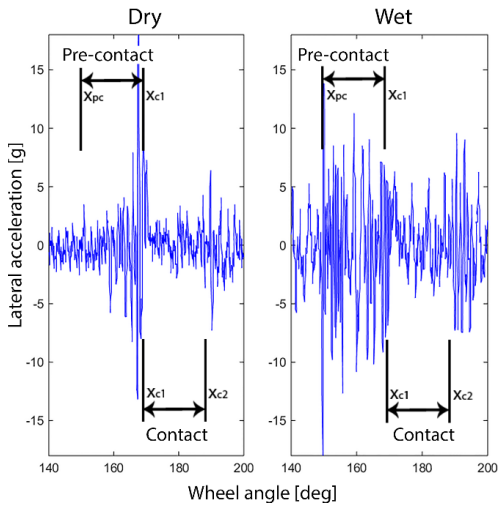

Figure 9. Pre-contact and contact sections marked in the raw lateral acceleration signal from dry and wet at 40 km/h.

Respectively, the indicator for the contact region vibration is integrated between the point x_{c1} and x_{c2}:

$$A_c = \int_{x_{c1}}^{x_{c2}} |y_{filt}(\varphi)| d\varphi \tag{3.2}$$

The indicators are then normalized by the driving speed to obtain comparable values. Threshold values are set for the indicators to separate dry and wet contact. The pre-contact indicator A_{pc} increases if there is water on the road exciting the tyre before the leading edge. The contact indicator A_c increases if there is a water layer between the tyre and the road. The latter can be used to recognize the full aquaplaning. The procedure for the determination of the tyre-road contact state is illustrated in Figure 10.

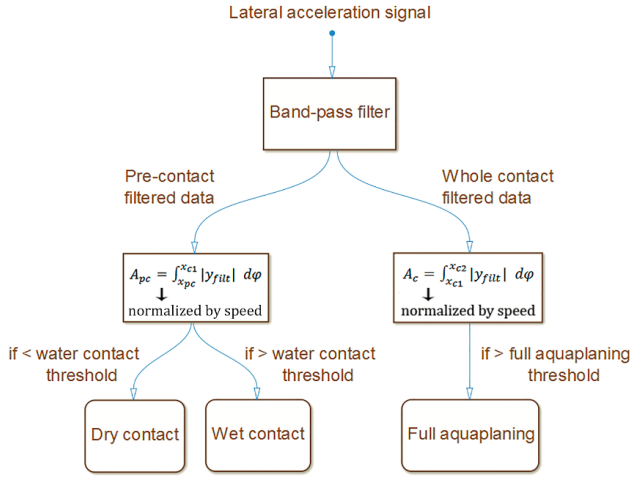

Figure 10. Procedure for the aquaplaning state determination.

3.3.3 Friction potential

To find the friction potential indicators on equally smooth surfaces, frequency analysis for the acceleration signals is applied in Publication [III]. In order to separate the friction related vibration components, the acceleration signal is first band-pass filtered. A lower frequency limit of 2 kHz and a higher limit of 5 kHz is used. As discussed previously, the tread vibration has been found to exist in the high frequency range. Discrete Fourier transform (DFT) is then utilized to obtain the power spectrum of the band-pass filtered signal. By integrating the area under the power spectrum curve, an indicator of friction potential is proposed.

The real road conditions and their effect on the acceleration signals provoke the need for more sophisticated frequency analysis method as is used in Publication [V]. The Hilbert-Huang transform (HHT) is a data-driven, empirical and adaptive analysis method for nonlinear and non-stationary data [39], [40]. It does not rely on any assumption of *a priori* determined function as the basis of the analysis like the traditional methods such as Fourier spectral analysis and wavelet analysis. The HHT comprises two steps: the empirical mode decomposition (EMD) and the Hilbert spectral analysis (HSA).

The EMD is utilized to separate band-limited components from the original signal consisting of multiple different oscillating modes. Thus, the original signal will be decomposed into intrinsic mode functions (IMF) which satisfy the requirement of having envelopes symmetric with respect to zero and having the same number of extrema and zero-crossings. The main purpose of the EMD is to ensure the Hilbert transform to be meaningful when applied to the IMFs.

The EMD process is illustrated in Figure 11. It starts by taking the original signal $x(t)$ and finding the extrema i.e. the local maxima and minima of the signal. Upper envelope $u(t)$ is created by connecting the maxima by a cubic spline. The lower envelope $l(t)$ is formed respectively by connecting the minima. The mean $m(t)$ of these envelopes is then subtracted from the original signal $x(t)$ and the result is assigned as the first proto-IMF $h(t)$. This proto-IMF will then be assigned as the original data and the process is repeated until a stopping criterion is fulfilled. This process is called sifting. The stopping criterion used for the sifting is based on the normalized squared difference between two consecutive siftings [39]:

$$SD = \sum_{t=0}^{T} \left(\frac{\left| h_{1(k-1)}(t) - h_{1k}(t) \right|^2}{h_{1(k-1)}^2(t)} \right) \tag{3.3}$$

When the criterion is fulfilled, the proto-IMF will be the first final IMF and is subtracted from the original signal and the result is treated as the original signal. The first IMF contains the shortest waveforms i.e. highest frequency components contained in the signal. Then the process is repeated until the last IMF is a monotonic function and no further IMFs can be decomposed.

The EMD has now resulted in IMFs containing band-limited components, which will form the original data when summed together. The IMFs can then be assigned with the HSA procedure, for which the following equations are adopted from [39].

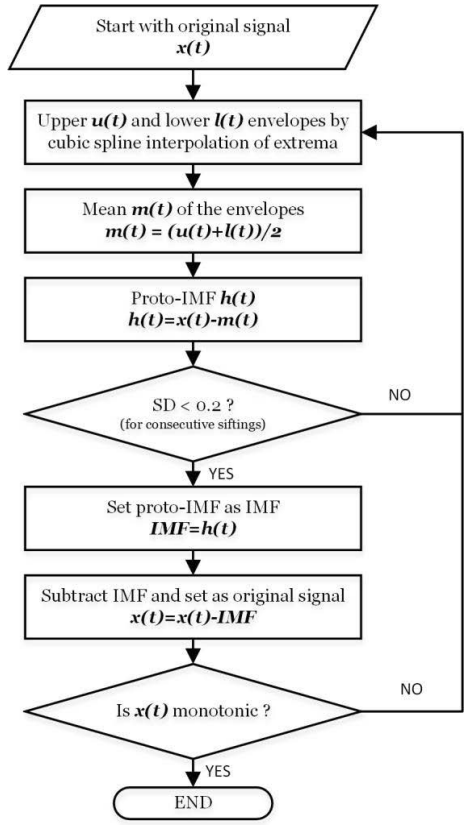

Figure 11. Empirical mode decomposition process.

HSA starts by applying the Hilbert transform which for a real valued signal *x(t)* is defined as:

$$H[x(t)] = \frac{1}{\pi} PV \int_{-\infty}^{\infty} \frac{x(\tau)}{t-\tau} dt = y(t) \tag{3.4}$$

where *PV* is the principal value of the singular integral. An analytic signal *z(t)* comprising the real valued signal *x(t)* and its Hilbert transform *y(t),* is defined as:

$$z(t) = x(t) + \mathrm{i}y(t) = a_{ins}(t)\exp(\mathrm{i}\theta(t)) \tag{3.5}$$

from which can be seen that the instantaneous amplitude $a_{ins}(t)$ and the phase function $\theta(t)$ are functions of time. These can now be presented as:

$$a_{ins}(t) = \sqrt{x(t)^2 + y(t)^2} \tag{3.6}$$

$$\theta(t) = \arctan\left(\frac{y(t)}{x(t)}\right) \tag{3.7}$$

The instantaneous frequency can then be derived from the unwrapped phase function:

$$\omega(t) = \frac{d\theta\,(t)}{dt} \tag{3.8}$$

The time-frequency-energy representation of the data is called the Hilbert energy spectrum and is defined as:

$$H(\omega, t) = Re \sum_{j=1}^{n} a_{ins,j}(t)^2 exp\left(\mathrm{i} \int \omega_j(t)\right) \quad (3.9)$$

It can be used to analyse the distribution of the energy of the IMFs in the time and frequency domain. This will be utilized with the accelerometer data to decompose different vibration components and to localize and detect especially the friction related vibration in the wheel angle coordinate. The time-domain data is transformed into wheel angle coordinate by utilizing the wheel encoder data. One wheel rotation is divided into 720 wheel angle bins in which the corresponding time-domain data is assigned. If multiple data points fall into a bin, the data points are averaged. The Hilbert spectrum is thus divided into 512 frequency bins with 50 Hz resolution and 720 wheel angle bins with 0.5 deg resolution. For plotting the results, 128 frequency bins are shown covering the frequency range of 0-6400 Hz.

3.3.4 Simplified flexible ring model

Various ring models have been utilized to study the deformation of a rotating tyre numerically. In Publication [IV], the tyre is modelled as a flexible ring connected by radial and tangential springs and dampers to the rim as shown in Figure 12, allowing deformation to tangential and radial direction (v and w respectively). A simplified flexible ring model solution with the following equations as presented in [41] is adapted. Following assumptions are necessary to reach computationally efficient solution for tyre-sensing applications especially without the knowledge of the external tyre-road interaction forces:

- The ring is assumed to be in-extensible (i.e. the circumferential length of the ring does not change) since modern tyre belts are extremely stiff in the circumferential direction. This results in following relation $w=-v'$ (the prime denotes a differentiation with respect to the rotation angle φ).
- In the contact, the deformation is assumed to follow geometric relations determined by the ring deforming against the flat surface.
- Outside the contact, the external forces are zero.

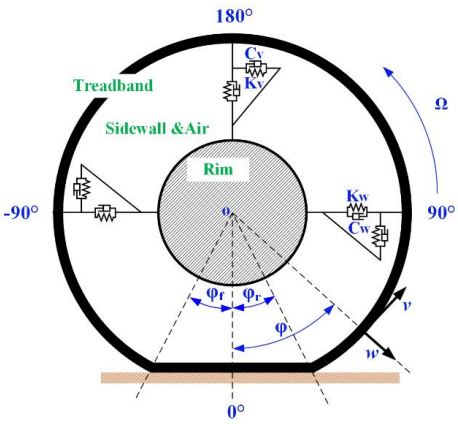

Figure 12. Flexible ring tyre model.

The variables describing the tyre properties are as follows:

- p_o inflation pressure
- a unloaded tyre radius
- b belt width
- c_w damping in radial direction
- c_v damping in tangential direction
- k_w spring stiffness in radial direction
- k_v spring stiffness in tangential direction

With the mentioned assumptions, the equation of motion outside the contact can be expressed as:

$$pw'' - c\Omega w' + (p - k)w = 0 \tag{3.10}$$

where p is the nominalized inflation pressure ($p_o a/b$), c is the equivalent damping (c_w+c_v) and k is the equivalent spring stiffness (k_w+k_v). The solution for (3.10) can be expressed as:

$$w = Ae^{\lambda_1 \varphi} + Be^{\lambda_2 \varphi} \tag{3.11}$$

Where:

$$\lambda_{1,2} = \frac{c\Omega \pm \sqrt{c^2\Omega^2 + 4p(k-p)}}{2p} \tag{3.12}$$

The radial deformation of the tyre outside the contact can be divided into two, the pre-contact w_f and after-contact w_r deformation:

$$w_f = Ae^{\lambda_1 \varphi} \tag{3.13}$$

$$w_r = Be^{\lambda_2 \varphi} \tag{3.14}$$

The radial deformation in the contact region is assumed to be governed by the geometric relations:

$$w_c = a - \frac{a-\delta}{cos\varphi} \tag{3.15}$$

where δ is the maximum radial deformation of the tyre. Following boundary conditions are set to satisfy the uniform behaviour at the leading and trailing edge:

$$w_f\big|_{\varphi=\varphi_f} = w_c\big|_{\varphi=\varphi_f}, \qquad w_f\big|_{\varphi=\varphi_f} = w_c\big|_{\varphi=\varphi_f} \tag{3.16}$$

$$\frac{dw_f}{ds}\bigg|_{\varphi=\varphi_f} = \frac{dw_c}{ds}\bigg|_{\varphi=\varphi_f}, \quad \frac{dw_c}{ds}\bigg|_{\varphi=\varphi_r} = \frac{dw_r}{ds}\bigg|_{\varphi=\varphi_r} \tag{3.17}$$

where $ds=(w+a)d\varphi$. With the boundary definitions, the following equations are derived:

$$A = \left(\frac{a-\delta}{\cos\varphi_f} - a\right) e^{\lambda_1 \varphi_f} \tag{3.18}$$

$$B = \left(\frac{a-\delta}{\cos\varphi_r} - a\right) e^{\lambda_2 \varphi_r} \tag{3.19}$$

$$\lambda \frac{a}{a-\delta} \cos\varphi + \tan\varphi - \lambda = 0 \tag{3.20}$$

The leading φ_f and trailing φ_r edge angles and can then be numerically solved. Thus, the radial deformation can be obtained and the acceleration profile based on the model derived.

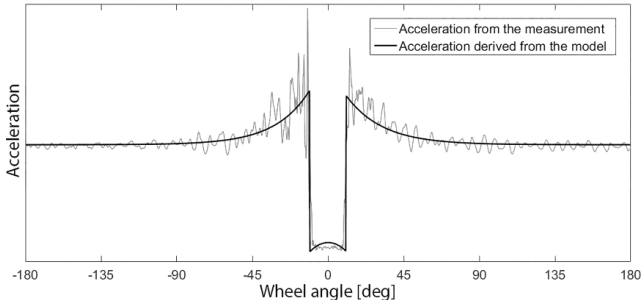

Figure 13. Radial acceleration derived from the model and the measured acceleration.

The acceleration profile is fitted to the measured acceleration data by utilizing a trust-region-reflective non-linear data fitting in the least squares sense. The estimated parameters are a, k, c, p and δ. Figure 13 shows an example of the acceleration profile derived from the contact deformation model fitted to the measured acceleration. The acceleration profile in the contact derived from the model shows curved shape as the pure radial deformation would produce. However, the sensor aligned with the road surface is not experiencing a change in the radial acceleration as visible from the measured signal.

4. Results and discussion

4.1 Aquaplaning

By utilizing methods described in section 3.3.1, a matrix of high-speed images overlayed with contact lengths calculated from the accelerometer measurements is obtained and shown in Figure 14. Results for three different tyre inflation pressures (1.8, 2.2 and 2.6 bar) and four different driving speeds (40, 60, 80 and 100 km/h) are shown. In the images, the leading edge of the tyre-road contact is on the right and the trailing edge is on the left. The green and red bars indicate the wet road contact and the hydrodynamic water contact respectively as introduced in section 3.3.1. These results were published in Publication [I].

At 40 km/h, the water contact does not produce a detectable peak and no indication of hydrodynamic region can be found. Contact length on the shoulder part (sensor 3, see Figure 14) is shorter than in the centre of the contact (sensors 1 and 2). This is due to the combination of slightly elliptic contact patch shape and the effect of the camber angle.

At 60 km/h, the road contact lengths slightly decrease and the hydrodynamic region becomes detectable. The red bars show the detected water contact well before the leading edge. The visual contact shape at the leading edge is straighter than in the case of 40 km/h. This is not observable from the accelerometer contact lengths.

At 80 km/h, the visual contact shapes from the images are highly distorted due to the water penetrating the centre part of the contact. The contact lengths measured with the accelerometers become more even and the shape is similar to the visual contact but not as pronounced.

At 100 km/h, there is still some form of visual contact in the images. However, the visual contact lengths are barely visible and can include a thin layer of liquid between the glass and the tyre resulting in negligible friction forces produced. The tyre is in full aquaplaning which results in detecting only the hydrodynamic region with the accelerometers.

In Figure 15, the contact lengths measured by the accelerometers 1 and 3 (the centremost and the outermost respectively) are plotted. The effect of the inflation pressure on the contact length can be observed at lower speeds. The lower pressure increases the contact length. When approaching the aquaplaning speeds, the contact lengths from the two sensors are clearly becoming more even. Very close to the full aquaplaning speed, the lower inflation pressure results in shorter contact length. The critical aquaplaning speeds, determined as

described in section 3.2, for different inflation pressures were 77 km/h (1.8 bar), 82 km/h (2.2 bar) and 89 km/h (2.6 bar).

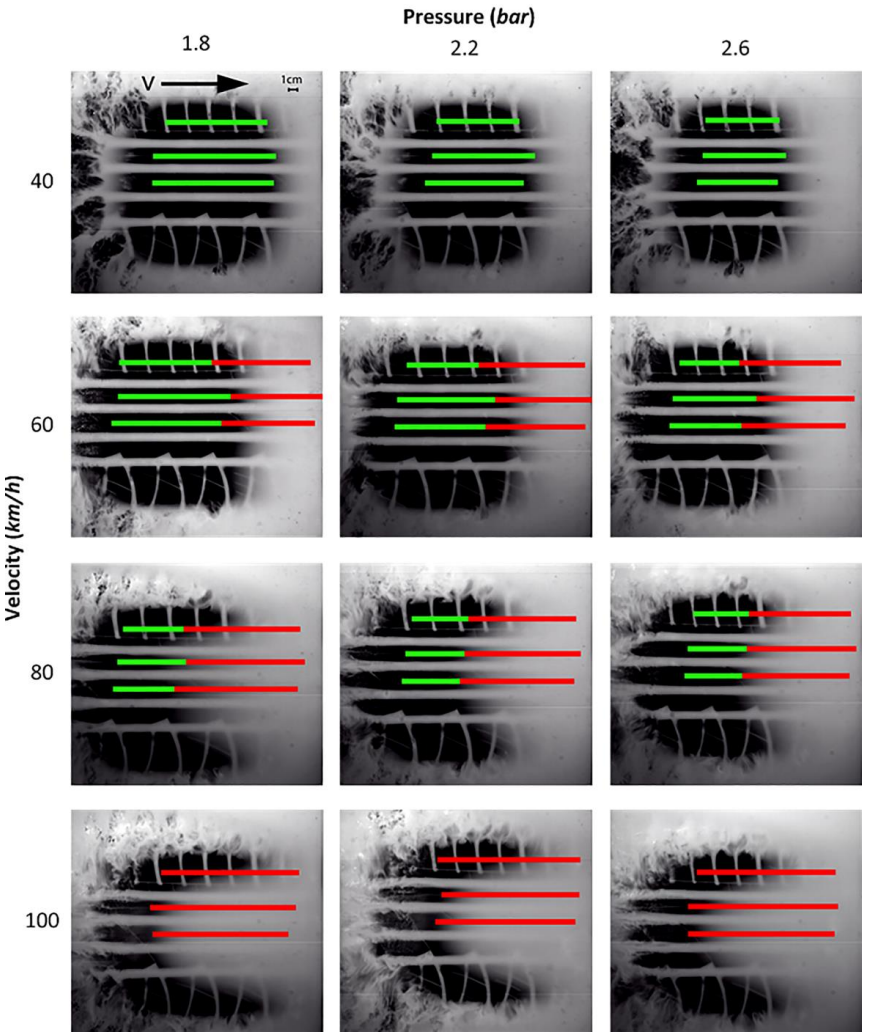

Figure 14. High-speed images and contact lengths from the accelerometer measurements (red bar: hydrodynamic aquaplaning, green bar: wet road contact).

4.2 Water detection

The results from the aquaplaning measurements were further analyzed with methods described in section 3.3.2. The detected contact lengths and the states of the wet contact by the proposed method are shown for four driving speeds in Figure 16. These results were published in Publication [II].

As can be seen at 40 km/h, the water contact is now detected from the lateral vibration. This was not possible with the pure contact length measurement as was shown in section 4.1. The method enables the detection of the water even if it has no impact on the actual contact length. Small layer of water can lower the friction coefficient significantly and thus it is in high priority to be detected. Up

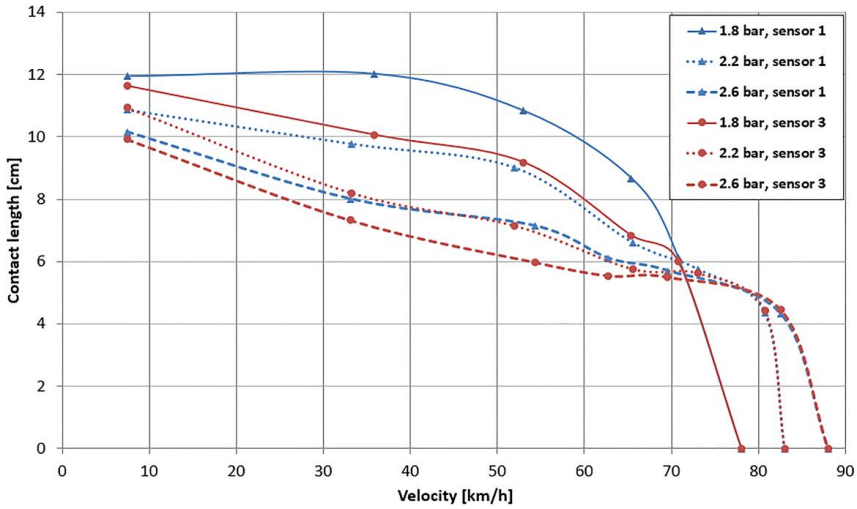

Figure 15. Contact lengths determined from the tyre sensors 1 and 3. The critical aquaplaning speed (i.e. contact length is zero) is defined by a separate measurement.

to 80 km/h, the pre-contact vibration indicates water contact but the contact section shows no signs of full aquaplaning. At 100 km/h, the indicator A_c increases due to the increased vibration throughout the contact. There is no actual tyre-road contact left and the tyre is lifted on top of the water layer. Thus, the state of the contact is determined as full aquaplaning.

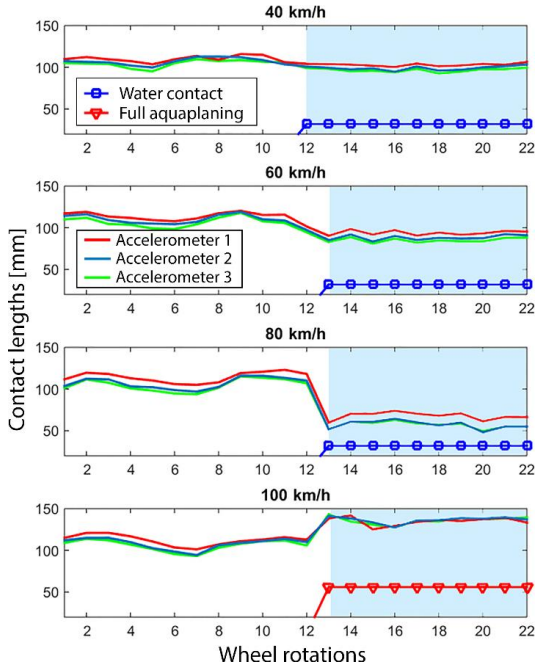

Figure 16. Contact lengths and the detected states of the wet contact detected by the method described in section 3.3.2. The white background indicates the dry asphalt and the blue background indicates the waterpool section.

4.3 Model-based approach

By utilizing a physical ring tyre model, described in section 3.3.4, a method to remove the acceleration profile caused by the contact deformation from the measured tyre sensor signal is introduced. In addition, the model parameters are estimated and the contact length information is obtained by fitting the model to the measured data. The data are obtained from the real road surfaces described in section 3.2. These results were published in Publication [IV].

The average values and standard deviations of the estimated model parameters for 10 tyre rotations at 40 km/h on different surfaces are shown in Table 1. It is clearly visible that the standard deviation of the parameters increase when moving from asphalt surface to ice and snow surfaces. This can be related to the fact that the contact boundaries are different for the low-friction and deformable surfaces than for the high-friction asphalt surface. The excitation from the asphalt remains rather stable whereas the slippery ice surfaces enable local sliding in the contact boundaries and thus the contact deformation varies slightly from one rotation to another. The effect of the snow surface is much more pronounced since the surface deforms under the tyre and the deformation of the tyre varies greatly.

Table 1. Average values and standard deviations of the estimated model parameters for 10 tyre rotations at 40 km/h.

Estimated parameter	Average				Standard Deviation			
	Asp.	*S. Ice*	*R. Ice*	*Snow*	*Asp.*	*S. Ice*	*R. Ice*	*Snow*
a [10^{-2} m]	31.04	31.00	29.91	30.15	0.34	0.78	1.01	1.28
k [10^{6} N/m^2]	12.2	13.1	13.2	12.5	0.66	1.44	2.38	3.34
c [10^{4} Ns/m^2]	2.27	2.54	2.87	1.21	0.58	0.82	1.44	1.77
p [10^{5} Pa]	14.9	15.1	14.9	15.6	0.061	0.087	0.198	0.54
δ [10^{-2} m]	2.56	2.61	2.56	2.69	0.06	0.09	0.15	0.26

The model parameters can be used to estimate the changes in operating conditions. One such application would be the detection of the loose surfaces (e.g. snow, gravel, mud) where the changes in contact deformation are significant. By averaging the estimated parameters throughout the normal operation of the tyre, the smaller changes could also be detected.

Table 2 shows the average values and standard deviations for the estimated contact angles (i.e. φ_r-φ_f). The contact lengths are then calculated by multiplying the time difference between the leading and trailing edge and the speed of the sensor (i.e. the speed of the wheel, zero-slip assumed for freely rolling tyre).

The contact lengths could be obtained reliably also for the snow surface, which poses difficulties with the traditional signal peak-seeking method. This is a great benefit since contact length estimate is one of the most interesting variable an intelligent tyre can provide. Reliably estimating the contact length under conditions creating fluctuations in the acceleration signal (e.g. road irregularities and loose surfaces) is of high importance. The deviation of the contact length again highlights the varying contact mechanism of the loose surface as discussed earlier.

Table 2. Average values and standard deviations of the estimated contact lengths and contact angles for 10 tyre rotations.

		Average				Standard Deviation			
	km/h	*Asp.*	*S. Ice*	*R. Ice*	*Snow*	*Asp.*	*S. Ice*	*R. Ice*	*Snow*
Contact length [m]	40	0.114	0.118	0.120	0.119	0.003	0.004	0.007	0.012
	60	0.114	0.117	0.118	0.126	0.004	0.002	0.003	0.005
	80	0.114	0.118	0.123	0.115	0.005	0.002	0.006	0.010
Contact angle [deg]	40	21.4	22.2	22.6	22.5	0.6	0.6	1.3	2.3
	60	21.5	22.0	22.2	23.8	0.6	0.4	0.5	1.0
	80	21.4	22.2	23.0	21.6	0.9	0.3	1.0	1.8

In Figure 17, the measured raw radial acceleration data and the estimated acceleration profile due to the contact deformation are shown. Also in the figure, the residual acceleration data when subtracting the estimated acceleration profile from the raw data are shown for the different surfaces. Each graph contains acceleration data from 10 tyre rotations. The estimated acceleration profile shown is the average from those 10 rotations and is used for visualization.

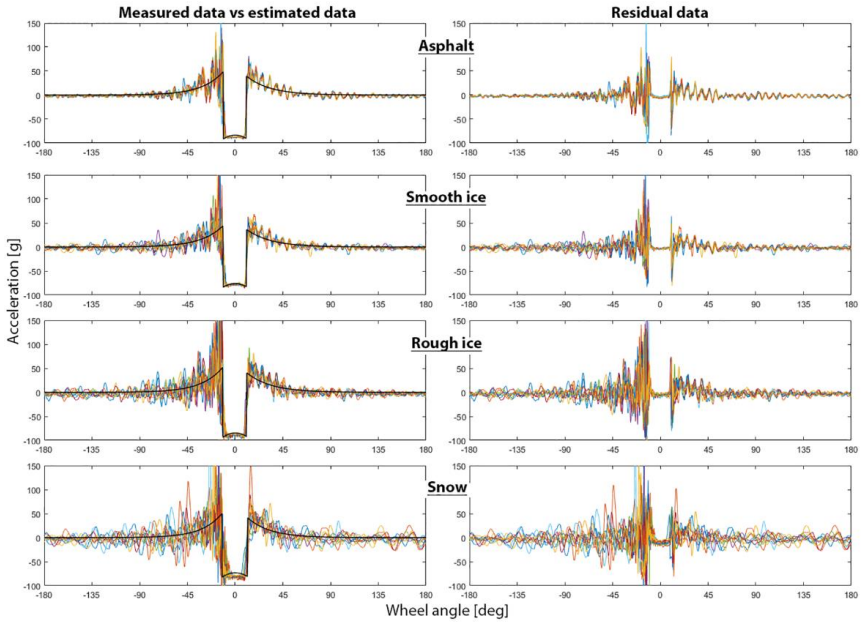

Figure 17. Measured raw acceleration data and the estimated acceleration profile caused by the contact deformation on the left. Residual acceleration data after subtracting the estimated acceleration profile on the right.

As can be seen from the residual data, the increasing and decreasing ramps caused by the deformation of the tyre are removed. This serves as a filtering method removing the effect of the contact deformation. The residual data can be used to analyse the acceleration data further without traditional filtering. Physical model-based filtering provides a way to process the data without losing any valuable additional information.

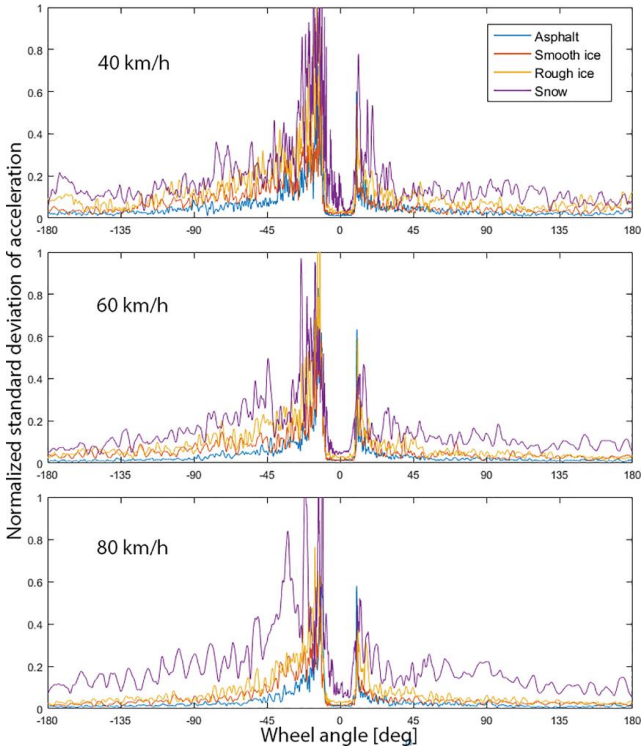

Figure 18. Normalized standard deviation of the residual acceleration for 10 tyre rotations.

In Figure 18, the standard deviation of the residual acceleration data is shown for 10 tyre rotations against the wheel angle. This provides a way to locate the regions with the most varying acceleration signal throughout the measurements on different surfaces.

The relative order of the deviation in the measured signals on different surfaces is clearly noticeable. The asphalt provides well-defined contact boundaries, as it is rigid and has high friction. Thus, it has the lowest deviation throughout the measurements. Smooth ice surface introduces lower friction level and thus more varying contact boundaries resulting in slightly increased deviation throughout the rotation of the tyre. Rough ice surface has more roughness than the smooth ice surface in addition to the low friction level. This results in even larger deviation. The snow surface results in clearly larger deviation than any other surface. As discussed earlier, this is a result of the high deformability, characteristic for the snow. This can also be detected inside the contact region, where other surfaces have relatively low deviation due to the flat contact containing no significant signal variation. On snow, the acceleration signal varies even in the contact resulting in an increased standard deviation. The tyre is not deformed against a rigid surface in this case and the contact patch can deform with the snow.

4.4 Tyre-road contact friction potential

For the tyre-road contact friction potential research, two different approaches were used. First, measurements were conducted on two equally macro-smooth surfaces with different friction levels to study the pure friction phenomenon and second, real road surfaces with different roughness, friction and deformability levels were introduced.

4.4.1 Equally macro-smooth surfaces

The two equally macro-smooth surfaces with different friction levels were chosen to study the pure friction related phenomena. The following results were published in Publication [III]. Figure 19 shows the raw acceleration signals measured on the smooth ice and concrete surfaces. The region of interest is the pre-contact part, framed in the graphs. The local sliding at the leading edge excites the tread and high-frequency vibration can be detected. The phenomenon is rather subtle and averaging over multiple rotations is needed to reliably detect such vibration. The excitation in the tangential and radial (X- and Z-axis respectively) direction is larger than in the lateral (Y-axis) direction and thus the measured vibration is more pronounced.

In Figure 20, a typical power spectrum for the band-pass filtered tangential acceleration signal is shown for the both surfaces. Due to the increased sliding-induced high-frequency vibration, the power of the signal is higher on ice than on the concrete. The area under the power curve was integrated and averaged for five tyre rotations on both surfaces. These averaged values of area under the curve for different tyre pressures and driving speeds are shown in Figure 21. For 20 and 30 km/h speeds on ice, the values are at least twice as large as on concrete surface for the tangential and radial acceleration. The lower excitation at 10 km/h speed reduces the measured vibration and the differences are not as large but still noticeable. The values on ice for lateral acceleration are larger than on concrete but the difference is clearly smaller.

By comparing the averaged values of the area under the power spectrum, an indicator for friction potential classification on equally macro-smooth surfaces is proposed. The increase in sliding-induced vibration at the leading edge is detectable on low-friction surface in the case of equally macro-smooth surfaces.

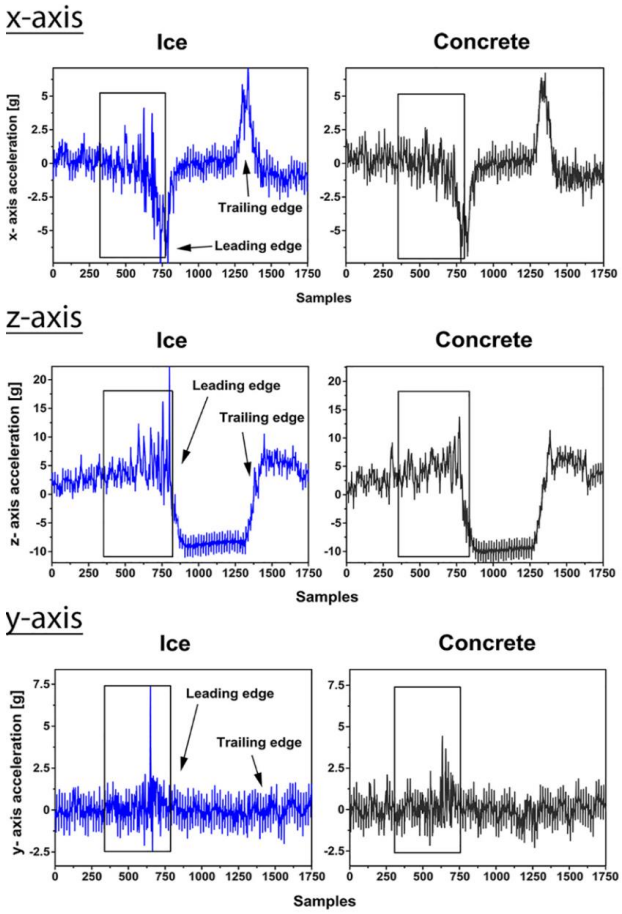

Figure 19. Acceleration signals from accelerometer 1 on ice and on concrete at 20 km/h (2.2 bar inflation pressure).

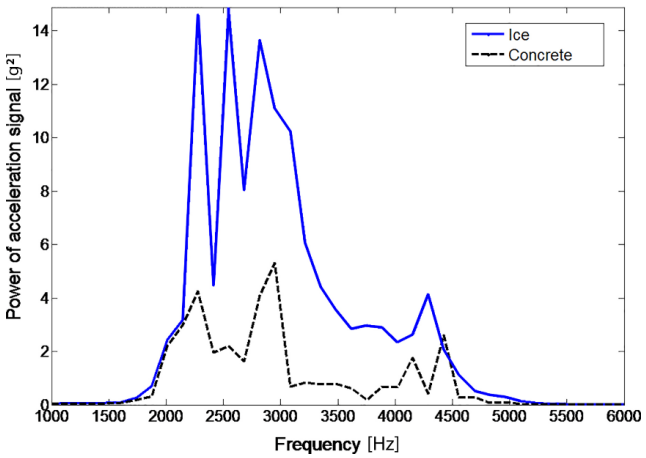

Figure 20. Typical power spectrum of the band-pass filtered tangential acceleration from equally macro-smooth ice and concrete surfaces.

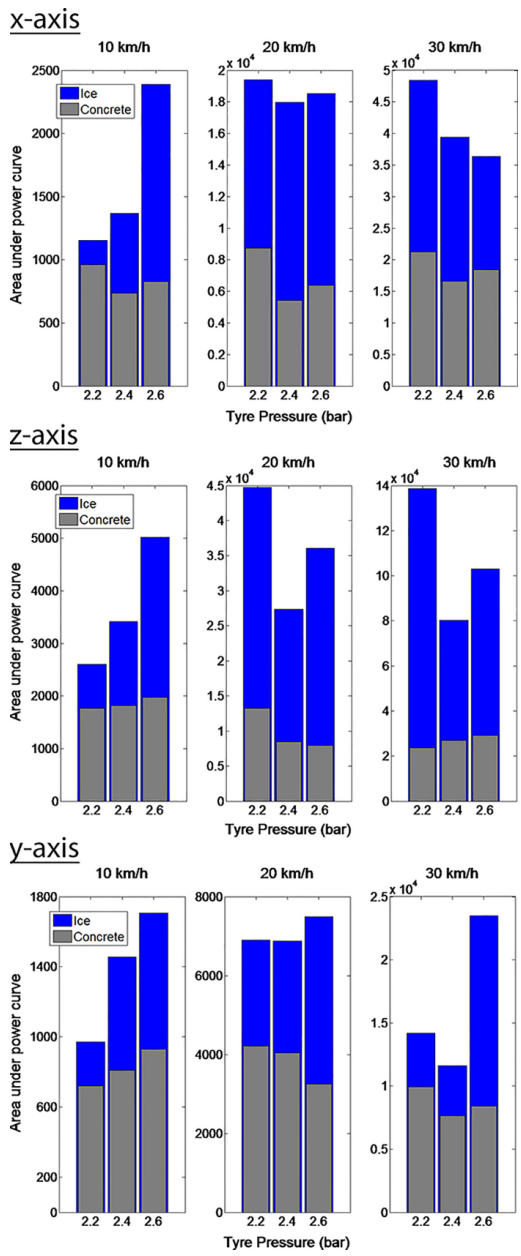

Figure 21. Average values for five rotations for the area under power spectrum of the band-pass filtered acceleration signals (accelerometer 1).

4.4.2 Real road conditions

In this section, the results from the measurements on real road conditions are shown and discussed. The following results were published in Publication [V]. As mentioned earlier, the introduction of the different roughness and deformability levels in addition to friction makes the detection of the local sliding more complicated. With equally macro-smooth surfaces, the leading edge vibration

could be related to the different friction levels. The leading edge vibration however, highly correlates with the surface roughness and the detection of the local sliding due to the low friction becomes complicated. By utilizing methods described in section 3.3.3, the following results were obtained on real road surfaces.

As discussed in section 2.1, the longitudinal shear stresses play important role in the tyre-road contact. The most interesting areas are the contact boundaries where the slip prone regions locate. Figure 22 shows the Hilbert energy spectra for the four surfaces, calculated from the first IMF of the tangential acceleration signal. The spectra are averaged from 15 tyre rotations. The vertical lines indicate the leading and trailing edges obtained by averaging the angle values from the 15 rotations.

By observing the trailing edge region, differences between the surfaces are detected. The energy of the vibration is distributed around the trailing edge on the both ice surfaces and on snow. In the trailing part of the contact, increased vibration is observable compared to the asphalt surface due to the local sliding of the tread rubber. On asphalt, the friction prevents the local sliding and the energy of the vibration is lower. The high-frequency vibration is concentrated right after the contact where the vibration excited by the contact deformation and the surface roughness occurs. The leading part of the contact also shows similar differences. The lower friction enables the sliding-induced vibration to occur also after the leading edge in the contact. This phenomenon is more pronounced in lateral acceleration signal as will be shown later. In the pre-contact part, the vibration is strongly dominated by the surface roughness.

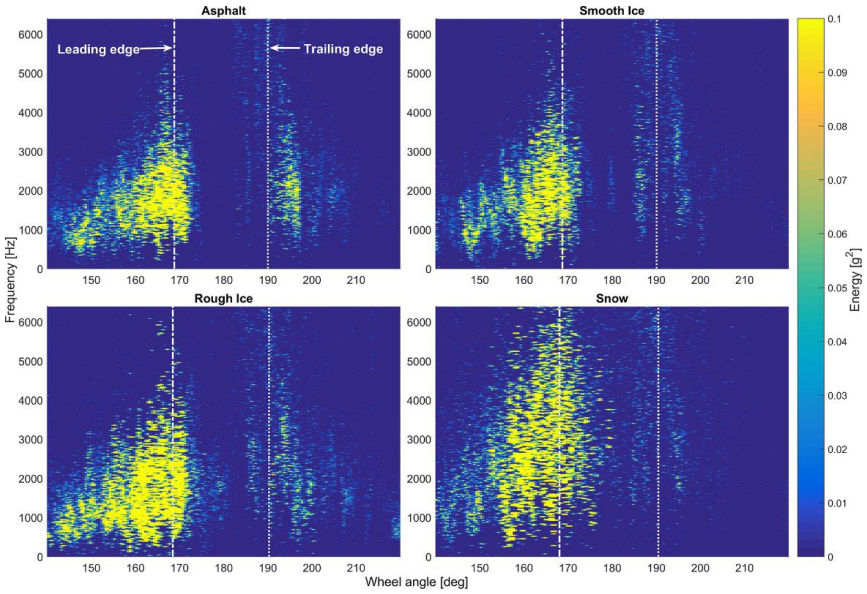

Figure 22. 5 x 5 Gaussian filtered Hilbert energy spectrum of the first IMF decomposed from the tangential acceleration at 40 km/h.

In Figure 23 (a), the energy of the vibration in the first IMF of the tangential acceleration signal is plotted for the 15 rotations separately. The energy is the

summed energy of the vibration from all the frequency bins at corresponding wheel angle. The wheel angle axis is zoomed around the trailing edge. As is now clearly visible, the surface roughness is a significant contributor also at the trailing edge. The energy of the vibration after the trailing edge is clearly higher on rough ice and asphalt surfaces. Inside the contact, the trailing part (area of interest) vibration can be again detected on low-friction surfaces. The snow surface is rather different from the three other surfaces as it is highly deformable. This results in significantly different contact mechanism exciting more the lower frequencies. The detection of the loose surfaces should thus be done by also considering the IMFs containing longer waveforms.

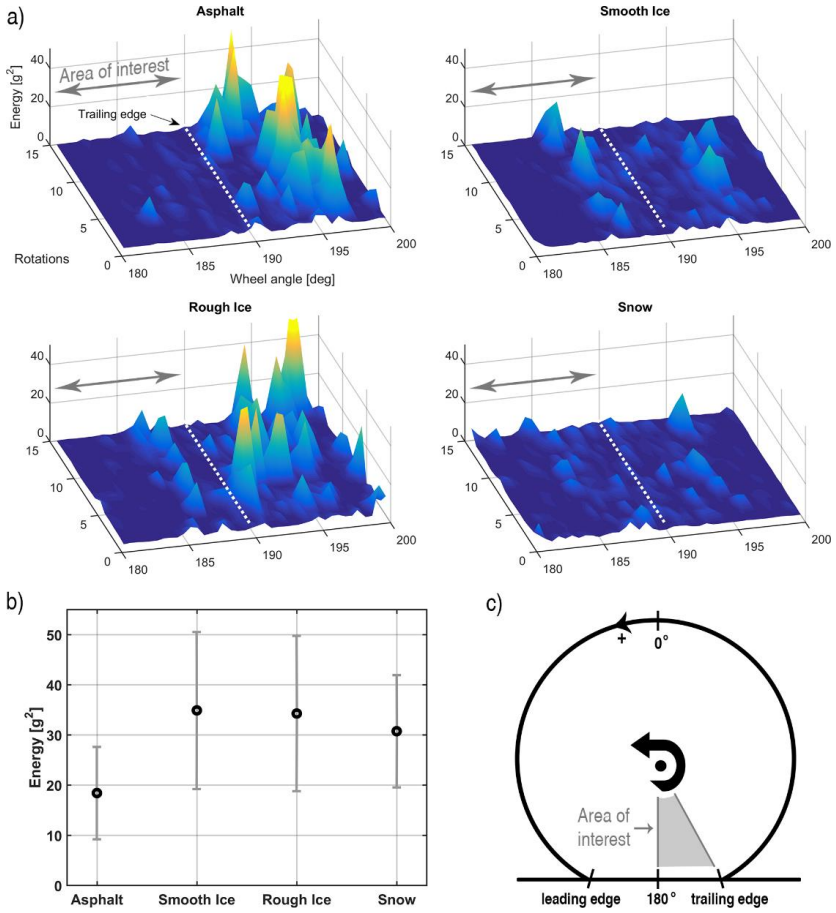

Figure 23. (a) The energy of the first IMF of the tangential acceleration in the trailing part of the contact for 15 rotations. (b) The mean values and the standard deviations for the summed energy of the first tangential acceleration IMF from 15 rotations in the trailing part of the contact (area of interest). (c) The coordinates used for the wheel angle information.

Figure 23 (b) shows the calculated mean values and standard deviations of the summed energies from the first IMF of tangential acceleration for 15 rotations. These values contain the summed energy from all of the frequency bins between the 180 deg wheel angle and the trailing edge (area of interest as shown in Figure 23 (c)). The energy of the vibration correlates with the friction level so that the

higher energy results from the lower friction. The friction coefficients for the surfaces were not measured and the relative order of the friction levels are based on observations during the measurements.

In Figure 24, similar Hilbert energy spectra are plotted as in Figure 22 but now for the first IMF of the lateral acceleration signal. As mentioned earlier, the local sliding is detectable also in the leading part of the contact, especially in the lateral acceleration. When observing the leading part of the contact (after the leading edge), higher energy of vibration can be seen on both ice surfaces than on asphalt. Once again, this indicates sliding-induced vibration rather than the surface roughness excited vibration. The snow results in widely distributed vibration energy due to the deformability of the surface similarly to the case of longitudinal acceleration. In the trailing part of the contact, the lateral acceleration does not indicate sliding-induced vibration, as was the case with longitudinal acceleration signal. The differences can be explained by the shear stress distributions in the contact. The longitudinal stress distribution is more prone to slip-regions at the trailing edge as was discussed in section 2.1.

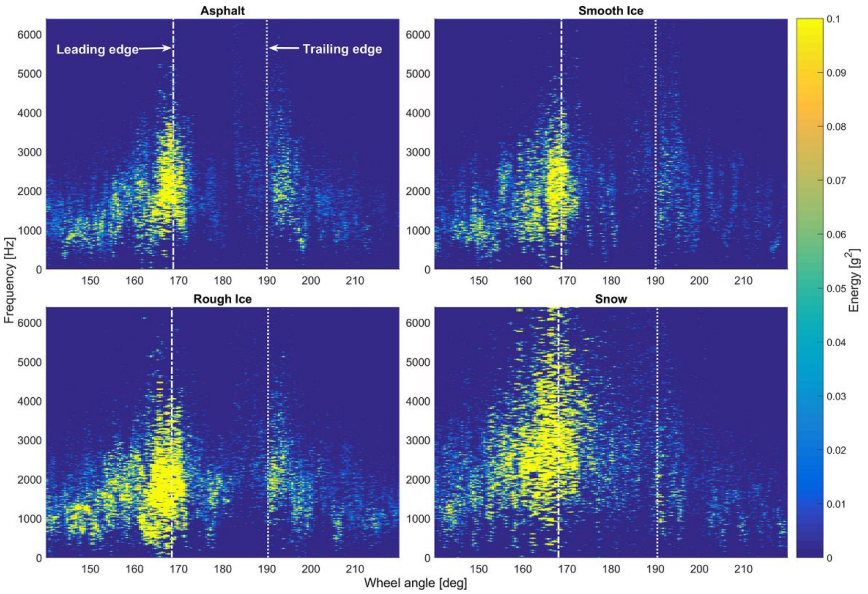

Figure 24. 5 x 5 Gaussian filtered Hilbert energy spectrum of the first IMF decomposed from the lateral acceleration. 40 km/h.

5. Conclusions

Intelligent tyres can provide vital information for many applications such as autonomous vehicles, advanced driver assistance systems, intelligent infrastructure and road monitoring. Moving from measuring what has happened in the tyre-road contact with the vehicle sensors to measuring what is happening in the contact is a fundamental change. However, interpreting the complex tyre responses and retracting the valuable information from the rotating tyre by fulfilling the vehicle safety standards at the same time is a demanding task.

In this thesis, accelerometers were used as tyre sensors to study the effects of aquaplaning and friction potential on the tyre inner liner response. In addition, a simplified flexible ring tyre model was used for the tyre sensor data interpretation.

For the aquaplaning measurements, traditional high-speed imaging on a liquid covered glass plate was conducted in addition with the accelerometer tyre measurements. These two methods were compared and following conclusions were made. The contact lengths and contact shape obtained from the acceleration signals showed generally similar distortions to high-speed images with different tyre pressures and driving speeds. The distortions from the sensor data were however smaller than the visual inspection of the images suggested. The difference is because the thin liquid layer and its transparency has a significant effect on the visual interpration whereas on the inner liner the major deformations are detected. The accelerometers could detect the initial contact with the water well before the critical aquaplaning speeds. This information can be utilized for the vehicle safety systems as well as for the tyre aquaplaning resistance research and development. The aquaplaning measurements were further analyzed and an algorithm capable of detecting the lateral vibration caused by the water contact was proposed. The method could detect the water in the contact at lower speeds than the pure contact length information suggested. In addition, the full aquaplaning could be separated from the dry contact, which was impossible for the pure contact length measurement.

The most important benefit the tyre sensors can provide for the tyre aquaplaning and wet grip research is the ability to be used on real road surfaces. This provides a way to measure the aquaplaning resistance of the tyres under realistic contact conditions and at the same time give more accurate information than the traditional braking and critical aquaplaning speed tests. The results related

to the aquaplaning studies in this thesis covered a comprehensive range of driving speeds and tyre pressures, which showed the potential of accelerometer tyre to provide valuable information under typical operating conditions.

The physical ring tyre model was used to estimate the acceleration profile caused by the contact deformation of the tyre. The model was fitted to the measured acceleration on different real road surfaces. The deviation in the model parameters obtained from the fitting suggested the different contact boundaries between the high-friction asphalt surface and the low-friction ice surfaces. The low friction enables sliding on the leading and trailing edge, which results in more varying contact. The snow surface resulted in significantly more varying contact since it is highly deformable and the contact conditions change throughout the rotation of the tyre. The parameter estimation could be used to detect smaller changes in the operating conditions of the tyre by utilizing long time averaging of the parameters. The contact lengths were reliably obtained from the estimation even on snow surface, which poses difficulties for the traditional signal peak-seeking methods. This is a significant benefit for the tyre sensing in real varying conditions. The estimated acceleration profile could also be used for physical model-based filtering. By subtracting the estimated acceleration from the raw signal, the effect of the contact deformation could be removed. The residual data can then be used for other tyre sensing purposes without valuable additional information lost in the filtering.

The effect of the friction potential in the tyre-road contact on the measured acceleration signals for freely rolling tyre were studied under different conditions. First, the effect of surface roughness was neglected by choosing equally macro-smooth surfaces with different friction levels. The smooth ice and concrete surfaces were used. By analysing the high-frequency components of the acceleration signal in the pre-contact region, an indication of the local sliding-induced vibration was found. The area under the band-pass filtered signal power spectrum was suggested as an indicator to differentiate the equally smooth surfaces with different friction levels. The most noticeable difference was found in the tangential and radial acceleration due to the largest excitation in these directions.

The effect of the friction potential was studied further on real road conditions. Four different surfaces with different roughness, friction and deformability level were used to differentiate the effects of these parameters. Hilbert-Huang transform was utilized to decompose and localize the vibration components in time-frequency domain. The HHT provides an effective signal analysis method for non-linear and non-stationary data. It is empirically based method, which can be modified in various ways. Thus, the interpretation of the results must be done in accordance with the utilized processing techniques. The IMFs were decomposed and the first IMFs containing the high-frequency components were analysed to detect the local sliding in the contact. The other IMFs are also useful for tyre sensing applications containing the tyre structural vibration and the effect of the contact deformation. By forming Hilbert energy spectrum, the local sliding-induced vibration could be localized. The energy of the tangential vibration in the trailing part of the contact was found to increase when friction decreases.

The roughness of the surface did not have effect on this vibration since the both ice surfaces (smoother and rougher than the asphalt) contained more energy than the asphalt surface. This was true also for the snow surface, however, the snow excites lower frequencies in the tyre and thus it should be detected from the IMFs containing longer waveforms. The detection of the tangential vibration in the trailing part of the contact can be explained by the longitudinal shear stress distribution where the slip-prone region is located near the trailing edge. The change in the shear stress direction during tread deformation at the trailing edge is also a contributor. The energy of the tangential and lateral vibration was found to slightly increase also in the leading part of the contact on low-friction surfaces. The low friction enables the local sliding when the tread comes in contact with the road surface. These high-frequency vibrations in the contact patch of a freely rolling tyre are low in amplitude and dampen quickly in the tyre rubber and thus pose challenges in the detection. The requirements for the accuracy and resolution of the sensor and related electronics are high since they also need to cover large amplitudes related to the contact deformation. The driving speeds covered in the results related to the friction potential were rather low and the tyre parameters were constant. Further work is thus suggested to cover wider range of operating conditions such as different tyres, inflation pressures, driving speeds and road surfaces. The results presented in this thesis have shown the possibility to detect the local sliding in the freely rolling tyre highlighting the potential of tyre sensing.

The effects of different driving manoeuvres on the measured accelerations were also studied. It was concluded that the lateral deformation of the tyre under steering was measureable. This could be utilized in lateral force estimation as suggested in the literature. Under braking on asphalt, the acceleration signal could clearly indicate the stick-slip regions in the contact patch. The progression of the slip region from the trailing part of the contact was noticeable under different slip ratios. Such accuracy provides possibilities for the accelerometer to be used in multiple tyre development tasks. On ice, the transition from the stick to slip was so quick that it was not possible to detect partial sliding. Under traction, the vehicle performance was limiting the obtainable slip ratios but the initial slip at the trailing edge was detected. In addition, the asymmetric deformation due to the braking and tractive forces were visible.

A limitation for the methods presented in this thesis and many other intelligent tyre applications is the limited execution and update time. It can be either the update rate from the sensor, which is once in one wheel revolution or the computational complexity of the algorithms that limits the use of these methods for example as a feedback for the ABS and ESC controllers. The methods can provide information for systems that utilize it at the update rate comparable to the sensor information. This includes updating the initial controller parameters before a needed manoeuvre based on the tyre-road contact information such as friction potential.

The accelerometer is a potential tyre sensor type providing information on multiple phenomena occurring in the tyre. The possibility to detect the local sliding in the tyre-road contact from the vibration of the freely rolling tyre being

the most intriguing. This paves the road towards the highly desired friction potential estimation. Further work is needed to study the multiple different operating parameters affecting the tyre sensor results. The possibility to measure the interesting underlying phenomena still needs to be validated for the various operating environments the tyre is facing. Accelerometers are small-sized and robust, which are essential requirements for a production tyre sensor. The power supply to the rotating tyre and the data transmission from the tyre are still significant challenges especially, if the required sampling rate is high. In addition, the development of robust methods to interpret the data in safety critical appliances is a challenge to tackle. To conclude, this thesis provided an insight to the possible applications and methods, which help to develop a tyre of the 21st century – an Intelligent Tyre.

References

[1] A. Lie, C. Tingvall, M. Krafft, and A. Kullgren, "The Effectiveness of Electronic Stability Control (ESC) in Reducing Real Life Crashes and Injuries," *Traffic Inj. Prev.*, vol. 7, no. 1, pp. 38–43, 2006.

[2] A. T. Van Zanten, R. Erhardt, G. Pfaff, F. Kost, U. Hartmann, and T. Ehret, "Control Aspects of the Bosch-VDC," in *International Symposium on Advanced Vehicle Control, AVEC'96*. pp. 573–607, 1996.

[3] S. Clark, *Mechanics of Pneumatic Tires*. Washington, 1981.

[4] European Union Parliament, "Regulation (EC) No 661/2009 of the European Parliament and of the Council of 13 July 2009 Concerning Type-Approval Requirements for the General Safety of Motor Vehicles, Their Trailers and Systems, Components and Separate Technical Units Intended Therefor." 2009.

[5] "Pirelli Connesso," 2017. [Online]. Available: http://www.pirelli.com/corporate/en/press/2017/03/07/pirelli-launches-a-beautiful-and-intelligent-tyre-at-the-geneva-motor-show-which-interacts-with-its-driver/. [Accessed: 14-Mar-2017].

[6] S. Clark, *Mechanics of Pneumatic Tires*. U.S. Department of Transportation, National Highway Safety Administration, 1981.

[7] S. Gong, "A Study of In-Plane Dynamics of Tires," Delft University of Technology, The Netherlands, 1993.

[8] M. G. Pottinger, "The Three-Dimensional Contact Patch Stress Field of Solid and Pneumatic Tires," *Tire Sci. Technol.*, vol. 20, no. 1, pp. 3–32, 1992.

[9] F. Liu, M. P. F. Sutcliffe, and W. R. Graham, "Prediction of Tread Block Forces for a Free-Rolling Tyre in Contact With a Rough Road," *Wear*, vol. 269, no. 9–10, pp. 672–683, 2010.

[10] J. Kidney, N. Mani, V. Roth, J. Turner, and T. Branca, "Experimental and Computational Studies of Contact Mechanics for Tire Longitudinal Response," in *Tire Society Conference*, 2011.

[11] Y.-J. Kim and J. . Bolton, "Effects of Rotation on the Dynamics of a Circular Cylindrical Shell With Application to Tire Vibration," *J. Sound Vib.*, vol. 275, no. 3–5, pp. 605–621, 2004.

[12] J. Périsse, "A Study of Radial Vibrations of a Rolling Tyre for Tyre–Road Noise Characterisation," *Mech. Syst. Signal Process.*, vol. 16, no. 6, pp. 1043–1058, 2002.

[13] O. J. Jousimaa, Y. Xiong, A. J. Niskanen, and A. J. Tuononen, "Energy Harvesting System for Intelligent Tyre Sensors," in *IEEE Intelligent Vehicles Symposium*, 2016.

[14] B. Breuer, U. Eichhorn, and J. Roth, "Measurement of Tyre/Road-Friction Ahead of the Car and Inside the Tyre," in *International Symposium on Advanced Vehicle Control*, 1992, pp. 347–353.

[15] T. Becherer, "The Sidewall Torsion Sensor System," in *2. Darmstädter Reifenkolloquim*, pp. 130–127, 1998.

[16] A. Pohl, R. Steindl, and L. Reindl, "The 'Intelligent Tire' Utilizing Passive SAW Sensors Measurement of Tire Friction," *IEEE Trans. Instrum. Meas.*, vol. 48, no. 6, pp. 1041–1046, 1999.

[17] J. Eom, H. Lee, and B. Choi, "A Study on the Tire Deformation Sensor for Intelligent Tires," *Int. J. Precis. Eng. Manuf.*, vol. 15, no. 1, pp. 155–160, 2014.

[18] R. Matsuzaki and A. Todoroki, “Wireless Strain Monitoring of Tires Using Electrical Capacitance Changes With an Oscillating Circuit,” *Sensors Actuators A*, vol. 119, pp. 323–331, 2005.
[19] A. J. Tuononen, “Optical Position Detection to Measure Tyre Carcass Deflections,” *Veh. Syst. Dyn.*, vol. 46, no. 6, pp. 471–481, 2008.
[20] A. J. Tuononen and L. Hartikainen, “Optical Position Detection Sensor to Measure Tyre Carcass Deflections in Aquaplaning,” *Int. J. Veh. Syst. Model. Test.*, vol. 3, no. 3, pp. 189–197, 2008.
[21] A. J. Tuononen, “Vehicle Lateral State Estimation Based on Measured Tyre Forces,” *Sensors*, no. 9, pp. 8761–8775, 2009.
[22] A. J. Tuononen, “Laser Triangulation to Measure the Carcass Deflections of a Rolling Tire,” *Meas. Sci. Technol.*, vol. 22, pp. 1–8, 2011.
[23] Y. Xiong and A. J. Tuononen, “The In-Plane Deformation of a Tire Carcass: Analysis and Measurement,” *Case Stud. Mech. Syst. Signal Process.*, vol. 2, pp. 12–18, 2015.
[24] Y. Xiong and A. J. Tuononen, “Rolling Deformation of Truck Tires: Measurement and Analysis Using a Tire Sensing Approach,” *J. Terramechanics*, vol. 61, pp. 33–42, 2015.
[25] Y. Xiong, “In-plane Tire Deformation Measurement Using a Multi-Laser Sensor System,” Aalto University, 2016.
[26] R. Matsuzaki, N. Hiraoka, A. Todoroki, and Y. Mizutani, “Optical 3D Deformation Measurement Utilizing Non-Planar Surface for the Development of an ‘Intelligent Tire,’” *J. Solid Mech. Mater. Eng.*, vol. 4, no. 4, pp. 520–532, 2010.
[27] T. R. Botha and P. Schalk Els, “Digital Image Correlation Techniques for Measuring Tyre-Road Interface Parameters: Part 2 - Longitudinal Tyre Slip Ratio Measurement,” *J. Terramechanics*, vol. 61, pp. 101–112, 2015.
[28] S. Vercammen, C. G. Díaz, P. Kindt, J. Middelberg, C. Thiry, and J. Leyssens, “Experimental Characterization of the Dynamic Behavior of Rolling Tires,” in *Proceedings of ISMA2012-USD2012*, pp. 1617–1628, 2012.
[29] T. Dare and R. Bernhard, “Accelerometer Measurements of Tire Tread Vibrations and Implications to Wheel-Slap Noise,” *Tire Sci. Technol.*, vol. 41, no. 2, pp. 109–126, 2013.
[30] M. Brusarosco, A. Cigada, and S. Manzoni, “Experimental Investigation of Tyre Dynamics by Means of MEMS Accelerometers Fixed on the Liner,” *Veh. Syst. Dyn.*, vol. 46, no. 11, pp. 1013–1028, 2008.
[31] M. Brusarosco, A. Cigada, and S. Manzoni, “Measurement and Analysis of Tyre and Tread Block Dynamics Due to Contact Phenomena,” *Veh. Syst. Dyn.*, vol. 49, no. 6, pp. 855–869, 2011.
[32] S. Hong, G. Erdogan, K. Hedrick, and F. Borrelli, “Tyre–Road Friction Coefficient Estimation Based on Tyre Sensors and Lateral Tyre Deflection: Modelling, Simulations and Experiments,” *Veh. Syst. Dyn.*, vol. 51, no. 5, pp. 627–647, 2013.
[33] R. Matsuzaki, K. Kamai, and R. Seki, “Intelligent Tires for Identifying Coefficient of Friction of Tire / Road Contact Surfaces Using Three-Axis Accelerometer,” *Smart Mater. Struct.*, vol. 24, pp. 1-9, 2015.
[34] S. M. Savaresi, M. Tanelli, P. Langthaler, and L. Del Re, “New Regressors for the Direct Identification of Tire Deformation in Road Vehicles Via ‘In-Tire’ Accelerometers,” *IEEE Trans. Control Syst. Technol.*, vol. 16, no. 4, pp. 769–780, 2008.
[35] D. Krier, G. S. Zanardo, and L. del Re, “A PCA-based Modeling Approach for Estimation of Road-tire Forces by In-tire Accelerometers,” in *Preprints of the 19th World Congress The International Federation of Automatic Control*, 2014, pp. 12029–12034.
[36] H. Morinaga, Y. Wakao, Y. Hanatsuka, and A. Kobayakawa, “The Possibility of Intelligent Tire (Technology of Contact Area Information Sensing),” in *FISITA World Automotive Congress*, 2006.
[37] H. Morinaga, Y. Hanatsuka, Y. Wakao, and Bridgestone Corporation, “Sensing Technology Tire System for Road Surface Condition Judgement,” in *FISITA World Automotive Congress*, 2010.

[38] Endevco Corporation, “Model 35A Isotron Accelerometer Datasheet,” 2017. [Online]. Available: https://www.endevco.com/product/prodpdf/35A.pdf. [Accessed: 19-Jan-2017].
[39] N. E. Huang *et al.*, “The Empirical Mode Decomposition and the Hilbert Spectrum for Nonlinear and Non-Stationary Time Series Analysis,” *Proc. R. Soc. London A*, vol. 454, pp. 903–995, 1998.
[40] N. E. Huang *et al.*, “A Confidence Limit for the Empirical Mode Decomposition and Hilbert Spectral Analysis,” *Proc. R. Soc. A Math. Phys. Eng. Sci.*, vol. 459, no. 2037, pp. 2317–2345, 2003.
[41] Z.-X. Yu, H.-F. Tan, X.-W. Du, and L. Sun, “A Simple Analysis Method for Contact Deformation of Rolling Tire,” *Veh. Syst. Dyn.*, vol. 36, no. 6, pp. 435–443, 2001.

Aalto-DD 129/2017

ISBN 978-952-60-7518-1 (printed)
ISBN 978-952-60-7517-4 (pdf)
ISSN-L 1799-4934
ISSN 1799-4934 (printed)
ISSN 1799-4942 (pdf)

Aalto University
School of Engineering
Department of Mechanical Engineering
www.aalto.fi

BUSINESS +
ECONOMY

ART +
DESIGN +
ARCHITECTURE

SCIENCE +
TECHNOLOGY

CROSSOVER

**DOCTORAL
DISSERTATIONS**